Matrix Isolation and IR Spectroscopic Study on Late-Transition Fluorides, Metal Oxo Complexes and Actinide Halides

Inaugural-Dissertation

to obtain the academic degree

Doctor rerum naturalium (Dr. rer. nat.)

Submitted to the Department of Biology, Chemistry, Pharmacy

of Freie Universität Berlin

by

Lin Li

Berlin

2021

The work for the present dissertation has been carried out between September 2016 and December 2020 under the supervision of Prof. Dr. Sebastian Hasenstab-Riedel and Dr. habil. Helmut Beckers at the Institute of Biochemistry, Chemistry, Pharmacy of Freie Universität Berlin.

First Referee: Prof. Dr. Sebastian Hasenstab-Riedel

Second Referee: Prof. Dr. Kallol Ray

Date of Defense: 16/04/2021

Declaration

I declare that this thesis was composed by myself, that the work contained herein is my own except where explicitly stated otherwise in the text, and that this work has not been submitted for any other degree or professional qualification except as specified.

Acknowledgement

First, I would like to give my gratitude to my supervisor, **Prof. Dr. Sebastian Hasenstab-Riedel**, for offering me the opportunity to work in his group and his continued patience and support during my Ph.D. project. Special thanks go to my mentor **Dr. habil. Helmut Beckers** for granting me such cheerful teacher-student relationship, for guiding me consistently from the start of my work, and for many important discussions, as well as for reviewing all my manuscripts and giving me valuable feedback. Many thanks go to **Prof. em. Lester Andrews** for giving me chance to work with him in part work of this thesis. I would like to thank **Prof. Dr. Kallol Ray** for his time and effort to assess my work as a second reviewer.

I would like to thank **Tony Stüker** for guiding me in theoretical calculation and his computational contributions for our papers. The same thanks I would like to give **Frenio A. Redeker** for his patient support in the experimental and practical part. Thanks to **Yan Lu**, who gave me a lot of help and kind care. I had many nice discussions with **Prof. Dr. Bing Xu**, **Dr. Hongmin Li**, **Dr. Yetsedaw Tsegaw** and **Gene Senges**, thanks them. I would give thanks to **Sofiya Kotsyuda**, **Tyler Gully** and **Patrick Pröhm** for their kind care and nice friendship. For **Dr. Simon Steinhauer**, **Dr. Mathias Ellwanger**, **Dr. Jan Hendrick Nissen** and **Marlon Winter**, I would like to thank them all for their kind advises and help. Many thanks to my **workgroup members** for such happy and friendly working atmosphere. I was very happy working with all of you.

Thanks to **Dr. Dirk Andrea** and his Ph.D. student **Tilen Lindič**, who provided me strong support and many helpful discussions from a theoretical point of view. Thanks to **Dr. Tobias Schlöder**, who helped me on quantum-chemical calculations a lot. Thanks to **Sudong Zhang**, who has done his internship of 4 weeks with me. Many thanks to the staff of **workshops** and **ZEDAT** (Zentraleinrichtung für Datenverarbeitung). Thanks also to the staff of **our institute** and **Ph.D. office** (Promotionsbüro 2).

Thanks to my **family** and **friends** support ever since. And I want to thank my boyfriend **Xiaofeng** for his strong and consistent support. I could not finish this thesis without them. Therefore, this dissertation is dedicated to them.

Abstract

High-valent late transition metal complexes bearing multiple bonded, terminal M−O groups persistently attract attention. They are reactive intermediates in various oxidation reactions, and in hydrogen and oxygen atom transfer processes. Additionally, due to their peculiar electronic structures they often show an electrophilic radical oxyl ($O^{\bullet-}$) character than that of a closed-shell terminal oxo ligand (O^{2-}). Many early transition metal complexes with multiple M−O bonds are common, however, oxo complexes of group 11 and 10 metals are rarely investigated due to experimental and computational challenges. In this work, the target molecules were synthesized by the matrix-isolation technique and characterized by infrared (IR) spectroscopy combined with quantum-chemical methods to analyze their electronic structures and harmonic frequencies.

The linear oxo monofluoride OMF ($C_{\infty v}$, ground electronic state $^3\Sigma^-$ for M = Au, Ag, and $^4\Sigma^-$ for M = Ni, Pd, Pt), the T-shaped oxo difluorides OMF_2 (C_{2v}, ground state $^2B_2$ for M = Au, Ag, and $^3A_2$ for M = Ni, Pd, Pt), and the planar oxo trifluoride $OPtF_3$ (C_{2v}, $^4A_1$ ground state) as well as the hypofluorite FOPdF (C_s) are observed and spectroscopically assigned. A contradiction reported by Wei et al. [Inorg. Chem. 2019, 58, 9796−9810] regarding the ground state of $ONiF_2$ has been solved experimentally (low-spin $^3A_2$ rather than high-spin $^5A_1$) by the observation of an additional stretching band. For OMF_2, the singly occupied antibonding π* orbitals show significant oxygen (2*p* orbital) character, and these M=O π-bonds show a gradual conversion from a covalent to an inverted ligand field case going from the oxo metal group 10 to group 11 complexes. The high spin densities at the oxygen atoms of these oxo compounds indicate their high oxyl radical character. According to a simplified three-electron π-bonding scheme the spin population at the oxo ligand increases with increasing covalence of the M=O bond, and further increases with inversion of the M−O π-orbital space. The trend from an ionic to a covalent and even to an inverted ligand field has been analyzed also for the isoelectronic linear species of group 9 (MF_2), group 10 (OMF) and group 11 (OMO).

High-valent nickel fluorides are strong oxidizing agents and often take part in fluorination reactions. However, there is no available experimental structural data and spectroscopic information about molecular NiF_3 and NiF_4. On the one hand, their high reactivity leads to challenges in their synthesis; on the other hand, their open shell nature and low-lying excited electronic states make quantum-chemical calculation more complex. In this work, the distorted tetrahedral NiF_4 ($^3A_2$, D_{2d}) and the planar NiF_3 ($^4A_2'$, D_{3h}) molecules were produced by the reaction of thermal evaporation and laser ablation of elemental nickel with F_2 and trapped in solid rare gas matrices (Ne and Ar). The similarities of the experimental M−F stretching bands of the high-valent 3*d* metal fluorides of Fe, Co and Ni were particularly instructive for their identification. Furthermore, the expected shortening and strengthening of the M−F bonds with increasing the metal oxidation states, which was experimentally observed for the binary fluorides of the 3*d* predecessors FeF_n and CoF_n (n = 1-4), was not observed for the higher nickel fluorides NiF_3 and NiF_4. Their weak Ni−F bonds and a considerable fluorine radical character make these fluorides to very powerful fluorination and oxidation reagents.

Uranium and thorium hydrides attract great interest due to 5*f* electron participation in their bonding. Owing to their high carcinogenicity, matrix isolation is an appropriate technique to synthesize and investigate the related species. In this work, isolated molecular HAnX and H_2AnX_2 (An = U and Th, X = Cl and Br) have been produced in solid argon using laser-ablated U and Th atoms with HCl and HBr. All these novel molecular species have been explicitly assigned based on characteristic isotopic shifts and quantum-chemical calculations. The analysis of Mulliken partition shows an increasing *f*-orbital participation in the H−An bonds of the HAnX (X = F < Cl < Br) molecules, while the opposite trend

was observed in the An−X bonds. Moreover, the *f*-orbital participation is found to be larger for the Th analogues. Interestingly, the U−H stretching frequency increases in the series HUF < HUCl < HUBr < UH, as less electronic charge is removed from the U−H bond by the less electronegative substituent. A similar trend is found for the Th counterparts.

List of Abbreviations

B3LYP	Becke 3-parameter Lee-Yang-Parr
BP86	Becke 1988 and Perdew 1986
CASSCF	complete active space self-consistent field
CASPT2	second-order multireference perturbation theory
CCSD(T)	coupled cluster singles, doubles and perturbational triples
DFT	density functional theory
ECPs	effective core potentials
EPR	electron paramagnetic resonance
HF	Hartree-Fock
IR	infrared
LMCT	ligand-to-metal charge transfer
LED	light-emitting diode(s)
M	metallic center(s)
MCT	mercury cadmium telluride
MRCI	multi reference configuration interaction
Nd:YAG	neodymium-doped yttrium aluminum garnet
OS	oxidation state
SI	supplementary information
SO coupling	spin-orbit coupling
SDD	Stuttgart/Dresden pseudopotential
T_{dopsit}	deposition temperature
TM	transition metal
UV	Ultraviolet
UV/Vis	Ultraviolet/visible

Contents

1. Introduction

The oxidation state (OS) concept is fundamental in chemistry because the valence-electron transfer can not be avoided in each redox reaction. These reactions play a central role in various chemistry fields, *e.g.*, catalytic process, biology, and material science. Based on this concept, compounds bearing elements in their highest possible oxidation states continually attract chemists; especially high-valent late transition metals (TM) are of current interest, because, due to their high formal *d* electron counts, they can reach the potentially highest possible oxidation states.

To obtain high-valent metallic centers (M), potent oxidizers are commonly used to react with late TM to produce intriguing oxides, fluorides and oxo complexes. The nature of the metal-oxygen chemical single or multiple bonds is also a focus to be attended. For example, the study of tetragonally distorted pseudo-octahedral complexes bearing terminal M=O group opens another important concept, the much-discussed concept about the existence of an "Oxo-wall". When the *d*-block metals are varied from left to the right, the nature of M=O converts from ionic to covalent and becomes eventually inverted in high-valent group 11 oxo compounds.

Great effort has been devoted to the investigation of TM oxo compounds experimentally and theoretically. However, those of the late TM are very rare, especially group 11 and 10 metal oxo complexes are to our knowledge still elusive.[1–3] For such compounds with late TM atoms, the difficulties stem from the experimental challenges and their difficult description by quantum-chemical methods. Their open-shell nature often produces several low-lying states, which makes it more difficult to determine their ground states. Hence, the chemistry of high-valent late TM oxo complexes is still underdeveloped.

1.1 Group 11 and 10 Metal Oxides, Fluorides, and Oxo Complexes

The series of experimental and theoretical studies focused on TM oxo complexes.[4,5] Group 11 and 10 metal-oxo complexes in particular have attracted special interest, *e.g.*, the activity of silver[6] and molecular gold complexes[7] as catalysts. Another frequently considered example is that of copper oxo complexes, as highly reactive intermediates that catalyze H-atom abstraction (HAT) and O-atom transfer (OAT) in biological systems. HAT and OAT reactions of oxo complexes of copper were attributed to a resonance between terminal $Cu^{III}O^{2-}$ and oxyl radical $Cu^{II}O^{\bullet-}$ intermediates (Figure 1.1).[1,8] However, despite the great effort has been put into this investigation, our knowledge of such intermediate complexes is still limited.[9]

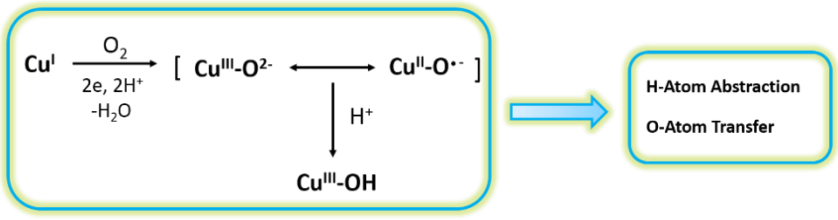

Figure 1.1. Proposed $[CuO]^+$ intermediates in H-abstraction and O-transfer processes.

Recently, computational studies and gas-phase experiments revealed an intriguing electronic structure of group 11 metal-oxo complexes.[1] For the bare diatomic $[CuO]^+$ cation the two unpaired π^* electrons

in the triplet ground state were found to have predominant oxygen *p* character, as shown by the spin population of 1.68 on O and 0.38 on Cu.[10] Also ligated $[LCuO]^+$ species predicted in various ligand environments were found to have a triplet ground state. Instead of a formal Cu(III) complex they are best described as Cu(II) oxyl species bearing oxygen centered radicals.[11] Consistent with their biradical character these species are found to be highly potent oxidants combined with a very low Cu−O bond energy. Similar results were predicted for the analogous $[LAgO]^+$ species.[12] It has been proposed that the oxygen *p* orbitals involved in π-bonding are higher in energy than the corresponding metal *d*-orbitals. And consequently, the π* orbitals show predominant oxygen ligand character. The oxygen ligands in such metal-oxyl $[M{-}O^{\cdot}]^{n+}$ species are oxygen-centered radicals.[3] However, strong experimental evidence of such intermediates continued to be rare. Both the low M−O bond energy and the high reactivity pose high challenges for the experimental investigation of such complexes. After the crystal structure of two terminal Au-oxo molecular complexes were erroneously reported, it was later found that these are tungsten analogues that have crystallized together with gold counterions.[13] Although it will be highly challenging to find an appropriate route to synthesize and investigate such late TM complexes bearing terminal oxo ligands, a great deal of effort is currently being made in this area. By studying the nature of such terminal M−O bonds (M = group 11), we can better understand their fundamental reactivity, and in particular their role in various biological and biomimetic oxidation reactions. Such insight will strongly support us in predictions and catalysis design.

It is also worth to get a deeper insight into the platinum group metal oxo complexes, due to their useful properties in catalytic conversion and oxidation catalysis.[14] For example, platinum is industrially used in the oxidation of ammonia to nitric oxide;[15] and palladium is used in the catalytic conversion of CO/NO_x to CO_2/N_2 and analogous processes for environmental protection.[16] In addition enzymes containing oxo species of nickel are frequently used in reactions as catalysis or intermediates.[2,3,9] However, the investigation of group 10 metal oxo species is still in its early stage, and only a few examples have been reported so far.[2,3,9] One reason for their high reactivity and low stability is the occupation of anti-bonding π* and even further σ* orbitals, which results in weakened M−O bonds. In addition, in late TM oxo complexes open-shell oxyl radical ligands ($O^{\bullet-}$) are preferentially formed instead of closed-shell oxido ligand (O^{2-}). In other words, from left to right in the *d* block series, the degree of oxyl radical character gradually increases associated with change from $M^{n+1}{=}O^{2-}$ to $M^{n}{-}O^{\bullet-}$.[2,9] It should be noted that these late TM oxo complexes do not break the well-known "oxo-wall" rule,[17] as we will describe later.

As the first stable group 10 oxo complex we mention here the Milstein complex, a platinum(IV)-oxo complex with strong proof from IR spectroscopy (shows an absorption at 783 cm^{-1} assigned to the Pt=O stretch).[18,19] The high-valent Pt^{IV} center is stabilized by a bulky pincer P−C−N ligand L (L = $C_6H_3[CH_2P(t\text{-}Bu)_2](CH_2)_2N(CH_3)_2$). The stabilization of oxo complexes containing high-valent late TM requires oxidation-resistant and sufficiently bulky donor ligands to shield and stabilize the highly electrophilic metal centre of a late TM oxo complex.

As for the nickel element, it is one of the most electronegative among the TM.[20] The most common oxidation states of nickel are 0 and II, and its highest known oxidation state is IV.[21,22] The first stable compounds described, carrying nickel in its highest oxidation state (IV) were consequently the solid hexafluoride $K_2[NiF_6]$[23–25] and the ternary oxide $BaNiO_3$.[26] Bright red $K_2[NiF_6]$ was obtained by fluorination of a mixture of KCl and $NiCl_2$ under strictly anhydrous conditions at 275 °C.[23] Such harsh conditions are essential, as the $[NiF_6]^{2-}$ anion is a very strong oxidizer which readily undergoes hydrolysis and generates dioxygen.[23] Black $BaNiO_3$ forms when $BaNiO_2$ is heated in an oxygen flow above 300 °C.[27] These compounds contain non-magnetic high-valent Ni ions in an undistorted octahedral ligand field.[24,25,28] Their vivid red and black color, respectively, indicate low-energy ligand-to-metal charge transfer (LMCT) optical transitions and highly covalent metal-ligand interactions as a result of a pronounced mixing of metal 3*d* and non-metal 2*p* valence states. Late TM in high oxidation states are strong oxidizers and the classical picture of predominantly ionic bonds in such an oxide is no more appropriate. For those oxides, where metal and oxygen valence states substantially overlap, a

substantial depopulation of the oxygen states ("holes" in the oxygen states) are expected.[29,30] For $BaNiO_3$ in particular, Mössbauer measurements are consistent with the existence of tetravalent nickel, while X-ray photoelectron spectroscopy (XPS) indicates a trivalent instead of a tetravalent nickel in this oxo metalation, suggesting a LMCT and the formation of oxygen anion holes in terms of the simplified description $Ba^{2+}Ni^{3+}(O^{2-})_2O^{\bullet-}$.[28]

In view of the fact that high-valent nickel oxides are widely used as catalysts for oxygen-evolution reactions[31] and as electrode material in electrochemical synthesis[32] and battery systems,[33,34] the question of the existence of Ni(IV) as an active species in these oxidic materials has been intensively investigated over the past 20 years.[34–37] Even if this question does not appear to have been finally solved,[34,36] the presence of tetravalent Ni(IV) in these materials was disproved in favour of Ni(III) and a reaction mechanism involving an active oxygen species.[35] Thus, the electrochemical oxidation of oxidic nickel(III) anode material likely produces electron vacancies on the oxide anion instead of an oxidation of Ni(III).[35] Due to a higher charge of the oxido group (O^{2-}) compared to a fluorido (F^-) ligand and in particular due to the higher binding energy of 2*p*(F) orbitals than that of 2*p*(O) orbitals (a consequence of the higher effective nuclear charge experienced by the 2*p* electrons of fluorine), orbital mixing between the 2*p*(L) and n*d*(M) orbitals is generally much smaller for L = F than for L = O. The 2*p*(O) orbitals are thus much more exposed to very strong oxidizing metal centers, and the oxidation potential of the metal cation can become high enough to draw electron density out of the 2*p*(O) orbitals, resulting in an oxyl ($O^{\bullet-}$) radical ligand.[29,30] Oxometallates bearing electrophilic oxyl radical ligands can become thermodynamically unstable with respect to the formation of peroxides, superoxides or finally the elimination of oxygen.[30,38]

Contrary to these anionic Ni(IV) compounds reports on binary charge-neutral high-valent nickel compounds such as NiF_3,[39,40] NiF_4,[39] and the elusive solid "NiO_2",[30] are very scarce. These apparently simple homoleptic Ni(IV) compounds are of interest because of their extreme chemical properties: solid nickel fluorides NiF_3 ($Ni^{2+}[NiF_6]^{2-}$ [39,40]) and NiF_4[39] are among the strongest known chemical oxidizers.[30] However, their use is limited by a low thermal stability, as NiF_3 decomposes thermally above 39-138 °C,[39] while NiF_4 already loses fluorine above –60 °C.[39] The thermally instable nickel fluorides were proposed to be the active oxidizing agent in the Simons process of the electrochemical fluorination using nickel anodes in anhydrous hydrogen fluoride, although there is still no clear spectroscopic evidence for this proposal.[41]

Higher oxidation states become progressively more stable when going down in the periodic table to the heavier 4*d* and 5*d* of group 10 metals.[22,42] The highest palladium oxidation state of IV is well established, *e.g.*: for the binary compounds PdO_2, PdF_4, and $[PdX_6]^{2-}$ (X = F, Cl, OH),[42] and platinum(V) and (VI) are well known in neutral binary fluorides such as the tetrameric, solid PtF_5,[43] and the mononuclear PtF_6.[44] Compared to the described ternary oxides and fluorides the synthesis of molecular high-valent Ni(IV) compounds can be an even bigger challenge due to their potentially high reactivity and low stability, as well as the absence of the electrostatic (Madelung) stabilization. Nevertheless, chemists have learned from the more stable organo platinum and palladium compounds,[21,45,46] and the recent chemistry of high-valent organo nickel compounds has uncovered a wealth of interesting chemical reactions, which is further proof that high-valent nickel compounds are still a current challenge and interesting targets in various areas of chemistry. Triggered by possible applications of high valent nickel compounds in organic catalysis[45,47] chemists have learned how to tame the extreme reactivity of highly oxidized nickel complexes by using appropriate oxidation resistant ancillary ligands that can lead to a substantial stabilisation of the formal Ni(IV) center, such as pyridine bases,[48] N-based tripodal scorpionate ligands like $(py)_3CH$ (tris(2-pyridyl)metane),[49] and $(pz)_3BH$ (trispyrazolylborat, Tp),[49,50] or N-heterocyclic carbene ligands.[51] Furthermore, bulky ligands which provide a steric protection to the metal center enabled the first synthesis of a tetra-coordinated organo nickel(IV) compound, tris(1-norbornyl)nickel(IV) bromide,[21,52] and only five years later the unexpected synthesis of a stable tetraalkyl nickel(IV) complex.[21,53]

One might wonder whether these organo-nickel compounds really contain high-valent nickel or whether they are complexes of Ni(III)/Ni(II) with partially oxidized ligands.[54,55] Indeed, such a redox non-innocent behaviour has recently been proved for a nitrogen (PNP) pincer ligand in the cationic square planar coordinated $[(PNP)NiCl]^+$ complex ([PNP = N(2-P(*i*-Pr_2)$_2$-4-methylphenyl]$_2$) by ligand K-edge X-ray absorption spectroscopy.[56] Another instructive example is the neutral formal Ni(IV) complex (Tp)Ni(aryl)$(CF_3)_2$ which was used in a cross-coupling reaction leading to a facile elimination of aryl−CF_3.[57] According to a recent computational analysis this complex is better described as a Ni(II) compound bearing a σ-non-innocent cationic aryl ligand.[58] While a conventional redox non-innocent ligand behaviour refers to ligand-centred π-orbitals,[54] σ non-innocence was more recently shown to be an intrinsic feature of high-valent late TM complexes.[38,54,58,59]

In addition to the experimentally well characterized and stable organo Ni(IV) derivatives, some very few low-coordinated nickel(IV) compounds are known. These are the molecular linear dioxide ONiO,[4,60,61,62] a bis(η^2-superoxide) Ni(III) cation $[Ni(O_2)_2]^+$,[63] and, very recently, the low-coordinated nickel oxofluoride $ONiF_2$.[64] Oxofluorides of the heavier congeners of Ni, Pd and Pt, have not been reported so far. These seemingly simple, low-coordinated Ni(III) and Ni(IV) compounds are of particular interest because the extreme reactivity and the high oxidative power of their high-valent Ni centers are not tamed by sterically protective or electron-donating ligands. More importantly, they are of remarkable simplicity, and thus ideal representatives for accurate electronic structure calculations (for representative calculations on organo Ni(IV) compounds see[58,65]). The linear dioxide ONiO ($^1\Sigma_g^+$) has been identified by matrix-isolation IR spectroscopy as a product of the reaction between Ni atoms and O_2.[4,60] It is also formed from nickel dust and oxygen in the earth mesosphere/lower thermosphere.[62] The bis(η^2-superoxide) Ni(III) complex $[Ni(O_2)_2]^+$ (^3A_g, D_{2h}) was studied by gas-phase IR photo-dissociation spectroscopy,[63] and the mononuclear oxofluoride $ONiF_2$ was part of a systematic study of the series of 3*d* metal oxofluorides by matrix-isolation spectroscopy and electronic structure calculations.[64,66,67] Interestingly, the linear oxo monofluoride, ONiF ($^4\Sigma^-$) has not been observed experimentally, and for $ONiF_2$ only the strongest Ni−F stretching frequency was detected experimentally in this previous study.[64]

1.2 Actinide Halides and Complexes

A special attention is paid to early actinide metal atoms and their reaction with halides, partly because of the involvement of the 5*f* electrons in the chemical bonds of their compounds. Particular interest was devoted to the investigation of uranium fluorides, which is related to the nuclear fuel cycle and the application of uranium metal. UF_6 is the most extensively studied uranium species. It has a regular molecular O_h structure with an electronic ground-state configuration $5f^0$,[68] and its U−F bond lengths were experimentally determined in electron diffraction studies to U−F = 1999(3)[69] and 1996(8)[70] Å. While much less data are available for UCl_6, the computed U−Cl bond length of the optimized O_h structure agree well with the bond length of its molecular structure in the crystal structure.[68] The optimized C_{4v} geometry of UF_5 was confirmed by its IR spectrum[71] with a $^2B_2$ ground state and one unpaired electron was accommodated in the $5f_{xyz}$ orbital.[68] The structure of UF_4 has been the subject of lively debate in the last 50 years, focused on whether it has a T_d or Jahn-Teller distorted D_{2d} symmetry. In its T_d structure, two unpaired electrons would reside in the f_{x3} and f_{y3} orbitals (t^2 configuration) which forms a triplet $^3T_1$ ground state.[68] Conclusions about the Jahn-Teller distorted D_{2d} structure of molecular UF_4 were reported by Bukhmarina *et al*., according to its IR spectrum in rare gas matrices.[72] However, from the theoretical calculation point of view, these two geometries are close in energy and produce very similar IR frequencies.[68] Recently, the crystal powder of UF_4 has been measured by X-ray diffraction and analyzed as *C2/c* space group.[73]

The reduction of UF_6 with NO_x produces UF_4, as originally described by Geichman *et al*.[73,74] Uranium metal will then be produced in an UF_4 reduction process and converted to uranium powder through UH_3, which is applied in the purification of uranium. UH_3 also reacts with HF to yield UF_4 at temperatures of 20-400 °C.[75] Therefore, the investigation of hydrofluorinated uranium compounds such as H_xUF_y is necessary to gain a better insight into possible intermediate products of these reactions. H_xUF_y have been investigated by matrix-isolation IR spectroscopy and high level (up to CCSD(T)/AVTZ) theoretical calculation.[76] The bonds of the bent $HU^{II}F$ molecule show significant ionic character. For the U−H bond, it has more than half percent *d*(U) orbital participation and also *f*(U) orbital contributions (U(69% *d*, 13% *f*); B3LYP/SDD/AVTZ).[76]

Due to similar chemical properties the corresponding thorium compounds were also studied as analogues related to uranium. A comparison of their electronic structures and spectroscopic properties allows a deeper insight into the nature and the differences in their chemical bonds. Different from linear UO_2 molecule, ThO_2 shows a bent structure due to the involvement of the 5*f* orbitals in the situation. Despite different size and energy 5*f* orbitals are also involved in the U−O bond, which nevertheless has a linear structure.

1.3 Objectives

The aim of this work was the detection and investigation of hitherto unknown molecular fluorides and oxo fluorides of the group 11 and 10 metals, as well as of novel hydridofluorides and hydridochlorides of the actinide metals U and Th. In particular, we aimed at the formation, the spectroscopic characterization, and the investigation of the electronic structures and the nature of the chemical bonds of the targeted compounds. In detail, the work consists of three parts.

First, to study the nature of M−O bond in group 10 and 11 metal oxo complexes. The comparison of low-coordinated OMF_2 (the 3*d* row, group 10 and 11) reflects trends in the bonding of the oxo ligand in these complexes. Electronic structure calculations on these oxo complexes can help to clarify the special bonding characteristics of late TM oxo complexes, particularly to gain knowledge on a possible redox non-innocent behaviour of the oxo group, and how these features develop with increasing metal-ligand covalency.

Second, to identify molecular NiF_3 and NiF_4, record their IR vibrational frequencies, and investigate their structures in the ground electronic states. In the series of high-valent 3*d* metal fluorides only the experimental M−F stretching frequencies of the molecular nickel compound are missing. To complete the list of the experimental IR frequencies of these fundamental molecular structures and their comparison is particularly instructive. Especially, the different nature of M−F bonds can provide valuable information about the reason for the powerful fluorination and oxidation ability of high-valent nickel fluorides.

Third, to investigate uranium and thorium halides. To get better understanding of the participation of 5*f* orbitals in the bonds of these small molecules. A comparison of experimentally observed and computed H−An (An = U and Th) stretching vibrations of a series of triatomic halides HAnX should provide insight into trends and the nature of their H−An bonds.

However, to the best of my knowledge, all these target compounds are instable under ordinary conditions. The compounds would be very reactive and rapidly undergo further reactions in the condensed state or in the gas phase. Therefore, in this work, the matrix-isolation technique was used to synthesize such elusive molecules, which can keep these highly reactive molecules isolated and stable in a solid noble gas host at cryogenic temperatures for recording their IR spectra and the investigation of their photochemistry.

1.4 The Matrix Isolation Technique

It is a potent technique developed by George C. Pimentel in the late 1950s,[77],[78] using host gas to form a matrix at low temperatures (< 20 K) and high vacuum (< 10^{-5} mbar) conditions. The method is based on trapping guest molecules in many cages separately and prevent them from reacting with each other molecules (cf. Figure 1.2). By this way, highly reactive species can be maintained even for hours, and their isolated state in an "inert" solid host reduce possible interaction with other molecules, which makes these conditions like "pseudo gas-phase" environments. Due to the cryogenic condition (near to absolute zero), rotational transitions are almost suppressed, and, apart from rare exceptions such as in the case of UO_2, [92] the isolated products reside in their electronic ground states. However, even though noble gases are widely used as host materials, they still interact with isolated guest molecules, leading to matrix shifts (called matrix effect), matrix sites, and noble-gas complex formation.

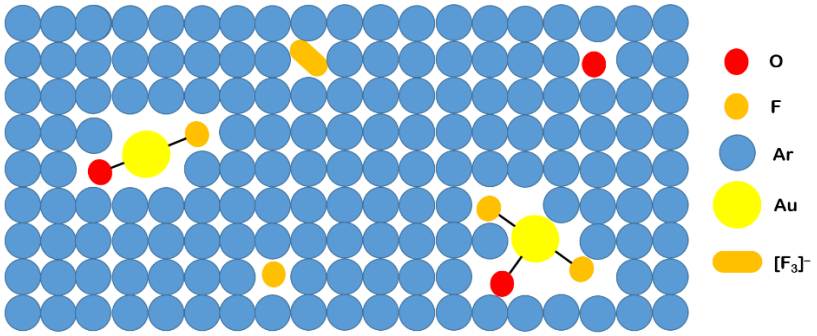

Figure 1.2. Schematic diagram of matrix isolated molecules.

The most common host gases are Ne and Ar, which were also used in the present work. Moreover, Kr, Xe and N_2 are often used as well. The choice of the host gas depends on the trapped guest molecules and depends on experimental demands. For example, neon is one of the most suitable matrix materials. Its transparency allowed for long-time deposition and render high-quality IR spectra possible. However, due to its low melting point sublimation of the solid matrix starts at temperatures above 10 K under the high vacuum conditions, which limits the temperature for annealing processes. The annealing process is an important method to let molecules rearrange and further low-barrier reactions to proceed. In contrast to Ne, a solid Ar matrix can be annealed above 35 K, making more reactions possible in an annealing process. The deposition temperature (T_{dopsit}) of an argon matrix can be varied between 6-20 K in order to improve the yield of a desired product in solid argon. However, Ar matrices are less transparent and show stronger interactions with guest molecules, which often reduces the spectral quality.

Different rare gases show different strength of interactions with the guest molecules, which is shown by the gas-phase to matrix shift, so-called "matrix effect", described as following:

$$\Delta\nu = \nu_{gas} - \nu_{matrix}$$

Stretching frequencies of matrix-isolated molecules are usually shifted to lower wavenumbers, and the strength of host-guest interaction for common matrix gases increases in the order Ne < Ar < Kr < Xe < N_2. In addition, reactive gases, such as pure F_2 and H_2, can also be used as matrix host for specific purposes. For example, pure F_2 is a kind of matrix gas used to produce elemental fluorides in high oxidation states,[79] and pure H_2 can facilitate metal hydrides formation and their dimerization.[80]

There are several techniques to generate and co-deposit guest molecules in noble gas matrices. For instance, compounds with sufficient volatility can be evaporated and co-condensed with excess matrix gas on the cooled matrix support. The easiest cases are stable gaseous samples; they can be directly diluted by host gas and co-deposited. If it is only stable at low temperatures, such as PtF_6, it can be

stored in a U-tube installed on the host-gas line in front of the matrix chamber. The host gas will guide the sample vapor into the matrix chamber where the mixture will be frozen on the cold matrix support. The vapor pressure of the guest molecule is controlled by the temperature of a cooling bath and the flowrate of the host gas. In addition, the Knudsen cell method and the laser-ablation technique can vaporize solid substances with low volatility, *e.g.* the Knudsen cell vaporize a solid by a heating filament, and the host-gas, flowing through the cell, carries evaporated molecules into the matrix chamber. The concentration of the molecules in the solid matrix is controlled by adjusting the power of the heating system. The advantage of the thermal decomposition is that it can be carried out essentially independently of the nature of the sample, *e.g.*, shape, hardness, and viscosity and so on. However, their melting point and thermal stability are important. For example, the high melting point of boron renders its thermal evaporation to be difficult, and substances with low thermal stability might decompose during heating. Moreover, for experiments with metal targets, like late TM in the present thesis, thermal decomposition can not efficiently form excited-state atoms and radicals. Therefore, the yield of compounds in high oxidation states is usually lower than using the laser-ablation technique.

In the present work, a focused high power laser beam was used to excite the metal targets. This technique is called laser ablation or pulsed laser sputtering.[81] The laser beam was shot on the bulk target with high energy, forming hot particles with a bright plasma, which will react further with gas mixtures and subsequently co-deposited on the matrix support. But due to the bright plasma radiation, photolysis of initially formed product molecules can not be avoided in the pulsed laser sputtering process, thereby affecting the detection of photosensitive products. Beside bulk substances, powder material also can be pressed as a target, such as green NiF_2 powder in this work. Anhydrous NaF, KF and CsF can be used as dopants for other substance targets, which has the advantage that the plasticity of the target increases, and anions are formed during laser-ablation.

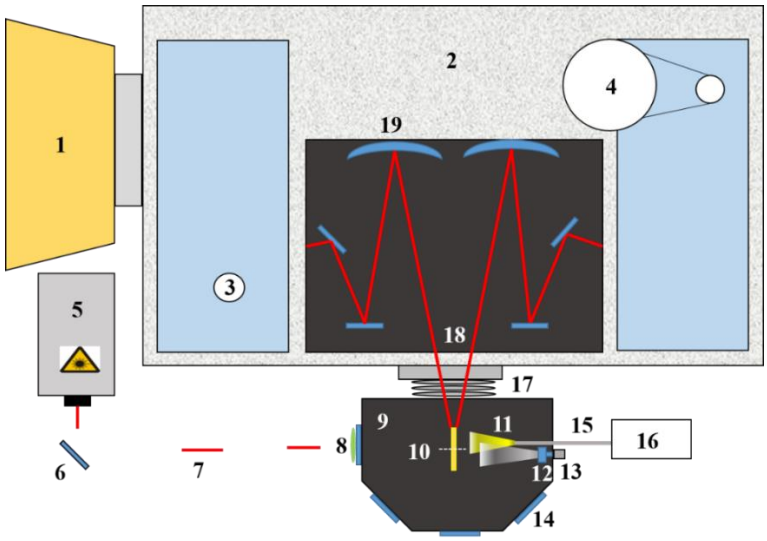

Figure 1.3. Matrix-isolation equipment combined with IR spectrometer. 1 Helium-cooled bolometer, 2 Fourier transform infrared (FTIR) vacuum spectrometer, 3 mercury cadmium telluride (MCT) detector, 4 interferometer unit, 5 neodynium-doped yttrium aluminum garnet (Nd:YAG) laser, 6 mirror, 7 laser beam, 8 focusing lens, 9 matrix chamber, 10 gold matrix support (dotted line: measuring position), 11 plasma, 12 target, 13 target motor, 14 quartz window, 15 matrix and reactant gas tube, 16 gas mixing line, 17 bumper, 18 IR beam, 19 transfer optic.

Figure 1.3 illustrates an experimental setup used in the present work. The bulk target (12) was installed on a rotating motor (13), which will ensure that the laser beam does not burn a single hole into the target, but rather a regular ring-shaped groove. The λ = 1064 nm laser fundamental of the Nd:YAG laser (5) is used with 7 ns pulse length and up to 50 mJ pulse energy (rate 1-10 Hz) and focused on the target surface (12) through a hole on the matrix support (10) by means of a focusing lens (8). The sputtered hot particles react further with reactant gas molecules prior to all gaseous products are frozen on the cold support

(10). The matrix support is a copper plate with a gold electroplate surface. It is also common to use IR transparent windows like CsI as the matrix support and to measure transmission IR spectra from the deposits. The reaction happens in the self-made chamber (9) at a high vacuum (10^{-7} mbar) and low temperature (6-20 K), by using the combination of an oil diffusion pump and a rotary-vane pump, as well as a cold head with a closed-cycle helium compressor system. The reason for using the oil diffusion pump instead of the more common turbo molecular pump is that elemental fluorine and chlorine are highly corrosive.

After co-deposition, the matrix can be annealed (Ne up to 10 K, Ar up to 35 K) by using a temperature controller (thermal energy). The annealing operation allows trapped molecules to relax in the cavities, which reduces the number of molecules in different matrix sites and facilitates the spectral analysis and subsequent irradiation experiments. LEDs, UV, and other light sources can be used for irradiation experiments via the quartz window (14). This is an important tool to initiate rearrangements, unimolecular decompositions, and bimolecular reactions of nearby trapped molecules, atoms, and radicals. The radiation can cause specific reactions of selected target molecules by using a selective wavelength of light. The rearrangement or decomposition of selected guest molecules facilitates the spectral analysis of complex mixtures and provides additional information about the species under study. The matrix support is rotatable, for irradiation experiments it needs to be turned by a 45° angle from the deposition position (as shown in Figure 1.3) to face window (14). For recording IR spectra, the matrix support needs to be turned anticlockwise in a perpendicular position to the IR beam (white dotted line in Figure 1.3).

Many kinds of spectroscopic methods can be combined with matrix isolation, such as IR, Raman,[82] ultraviolet and visible (UV/Vis),[83] and electron paramagnetic resonance (EPR)[84] spectroscopy. IR spectroscopy (2) is most commonly used, as a rapid and sensitive method providing many structural information. It was also used in this thesis. IR laser beam (18) is focused on a L-N2 cooled MCT detector (4000-350 cm^{-1}, (3)), and directed onto the matrix support by a transfer optic (19). For FIR measurements below 600 cm^{-1}, a helium-cooled bolometer (1) was used and the beam-splitter in the interferometer unit (4) needs to be adjusted as well.

Volatile samples can be placed in front of the matrix chamber in a cooled U-tube or cylinder in position (16), which can protect the sample from decomposition or from reacting with impurities in the gas-mixing line. For this purpose, the gas mixing device shown in Figure 1.4 was designed.

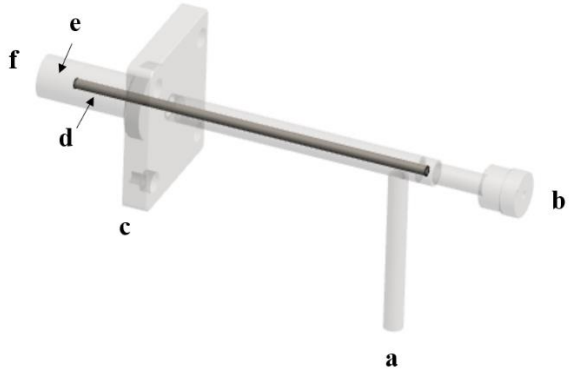

Figure 1.4. Schematic diagram of a stainless-steel gas mixing device.

This unit is designed for injecting extremely reactive volatile samples, such as PtF_6 and IrF_6. The cylinder is placed in a cooling bath and connected at position (**a**) (see Figure 1.4). The host gas tube is connected at position (**b**), where an O-ring seal is used to ensure airtightness. The host gas can be doped with another reactant gas, directed through the inner tube (**d**), and mixed with the precursor vapor

exclusively within the small cavity (**e**) just in front of the matrix support (**f**). The adapter (**c**) is installed at the matrix chamber instead of the matrix and reactant gas tube (15).

The quality of the obtained IR spectra depends on several independent factors, such as the concentration and the flow rate of the reactant gas/matrix gas mixture, the laser energy in laser ablation experiments, and the deposition temperature. In experiments carried out in this work laser-ablated metal atoms react with the reactant gas OF_2 (reactive gas diluted by noble gas) in the plasma zone (11) or during the deposition process on the cold surface of the matrix support.

The reactant concentration of the matrix gas mixture used in the present work was 0.01%-1% (Ne matrix) and 0.5-1% (Ar matrix). To achieve an IR transparent Ne matrix, lower concentrations and longer deposition time were usually successful. However, argon matrices can often not be improved by using longer deposition time, therefore higher reactant gas concentrations are recommended. Moreover, experiments with different reactant concentration are always recommended, to obtain additional concentration dependent information for the spectral analysis. For instance, some unstable species may only be produced in low concentration experiment, while higher concentration can increase the yield of higher coordinated product species and of larger complexes. The observation of such trends will provide additional proof for the spectral assignment.

The laser energy affects the amount of substances which are laser-ablated. It should therefore also vary corresponding with the reactant gas concentration. In the ablation of metals higher laser energy will produce more hot metal atoms but will also lead to a brighter broad-band radiation from the plasma plume. When photosensitive products are expected, this latter factor should be considered. The flow rate of the reactant/matrix gas mixture should also be varied during an experiment, since high flow rates result in rough matrix layers and spectra with bad quality.

Except for H_2 and Ne matrices, other common host gases can be deposited at temperatures of > 10 K. Higher T_{dopsit} favours the formation of the most stable products, while extremely unstable products may probably disappear from the spectrum. Therefore, after a suitable adjustment of the other parameters mentioned above, one could make an attempt with different T_{dopsit}.

1.5 The Role of Quantum-chemical Methods

In this work, computational methods are used for valuable predictions of vibrational frequencies of the novel species. Density functional theory (DFT)[85] calculations are often useful methods, because they are often less time consuming, require minimal computer resources for small molecules, and provide approximate structures and vibrational frequencies. DFT calculations were performed using the Gaussian[86] and the TURBOMLE[87] programs packages. Moreover, the MOLPRO[88] *ab initio* program was employed to deal with high-accurate calculations. In principle, ORCA[89] is suitable for almost all spectroscopic studies, while with late TM atoms its performance is not as perfect as it should be.

Frequently used DFT functional in the present work are B3LYP (Becke 3-parameter Lee-Yang-Parr)[90] and BP86 (composed of the Becke 1988 exchange functional and the Perdew 1986 correlation functional).[91] They provide approximate structural and thermochemical parameters for molecules with a single-reference electronic structure and reasonable predictions of their vibrational spectra. However, DFT methods are not reliable on identifying the ground electronic states of TM complexes with low-lying excited electronic states, especially when late TM atoms are involved. Therefore, accurate *ab initio* calculations are necessary for these predictions, such as coupled cluster calculations, based on restricted Hartree-Fock (RHF) theory, with full treatment of single and double and perturbative triple excitation (CCSD(T)), the so-called "gold standard of quantum-chemistry".[92] However, when low-lying excited states can not be neglected, multi-reference problems arise in CCSD(T) calculations with the T_1 diagnostic value higher than 0.05.[93]

The term "multi-reference character" refers to the fact that more than one orbital configuration needs to be considered in a correct description of the electronic structure of the molecule. When low-lying excited states have to be taken into account, multi-reference methods are required. In the present work, complete active space self-consistent field (CAS(*n*,*m*)SCF) calculations were carried out with an active space of *n* electrons in *m* orbitals in those cases where single-reference methods (DFT, CCSD(T)) can not be used. CASSCF only accounts for static correlation, and further treatment of dynamic correlation is included in second-order multireference perturbation theory (CASPT2).

As mentioned above, 4*d* and 5*d* metal elements are involved in this work. For that reason, relativistic effect needs to be considered in their accurate quantum-chemical description. Such relativistic effects arise as a result of an increased kinematic mass due to the high velocity of core electrons, thereby lead to a contraction of the related orbitals (direct relativistic effect) and a higher shielding of the nuclei (indirect relativistic effect). Due to the increased shielding, the indirect relativistic effect results in an expansion and destabilization of the outer orbitals (*d* and *f*, as well as outer $p_{3/2}$), which outweighs the direct effect. In turn, this destabilization of the outer valence orbitals stabilizes the inner next shell *s* and *p* orbitals. The effect accumulates with the increasing number of *d* electrons and partially explains the relative stabilization of group-11 Au, so-called "gold-maxium".[94] The effect leads to a 17.3% contraction for Au and directly relates to its ground state electron configuration ($d^{10}s$).[95] On the other hand, the relativistic effect increases the interaction between the electron spin and the orbital angular momenta, the spin-orbit (SO) coupling. This effect can not be neglected for elements heavier than nickel, since for higher angular momentum orbitals the interaction between orbital and spin magnetic moments is pronounced and results in a splitting of energy levels.

In practice, several possible approaches can account for relativistic effects, such as the Douglas-Kroll-Hess Hamiltonian (DKH, denoted as DK) [96] and the Zeroth-Order Regular Approximation (ZORA)[97]. Beside them and most common is the use of effective core potentials (ECPs), which is the main method also used in this work. The advantages of ECPs, on the one side, is that relativistic effects are taken into account, and, on the other side, the nuclei and the electrons close to nuclei are treated as core potential of the nuclei, thus simplifying the calculation.

1.6 Basic Concepts Relevant to this Work

High Oxidation State

Before discussing how to obtain high-valent TM compounds, we are required to find a proper definition for the term oxidation state. It's well known that the simple rules[98,99] for the estimating the formal oxidation state work quite well for ionic compounds. Specifically, in a TM compound, the bonding electron pairs between the ligands and the metal center will be counted for the more electronegative atoms, usually the ligands.[98,99] However, when it comes to redox-active "non-innocent" ligands[98], or to an "inverted ligand field"[38] case, the estimation of an oxidation state becomes more complicated. In such cases, the formal oxidation state more often shows significant difference with the actual electron distribution. That is also the reason why in TM complexes, the configuration d^{n} is more often used to describe the M center instead of the formal oxidation state.[100] Therefore, in this work, when we discuss oxidation state, we mainly focus on the actual electron distribution between the metal center and the ligands.

To obtain high possible oxidation states (OS), on the one hand, highly electronegative ligands are necessary to stabilize the metal ion. On the other hand, low ionization energies and a large number of valence electrons would facilitate high metal oxidation states. In principle, the highest oxidation state of a TM can be obtained with the maximum number of singly bonded most electronegative ligands such as fluorine, however, increasing the number of such ligands also increases both, the steric repulsion between them, and the Lewis acidity of the metal center. Thus, most highly fluorinated TM complexes

form stable anions or non-volatile solids. Moreover, less electronegative ligands can be more easily oxidized by a high-valent metal center. Therefore, terminal oxo ligands with a valence of up to three and a negative OS of up to –II combined with monovalent fluorine ligands appear to be a promising concept for the generation of high-valent molecular late TM compounds.

Unsurprisingly, the highest oxidation state so far experimentally achieved for a molecular system is the OS = IX, in the cation $[IrO_4]^+$.[101] In this case, the oxo ligand displayed the formal OS = –II. As such, the oxygen ligand might be a suitable candidate to obtain a metal center in high oxidation states without the effect of steric crowding.[102] Hence, the dication $[Pt^{+10}O_4]^{2+}$ could be a promising candidate for a metal center with the principally highest OS = +X.[103] However, it has been theoretically confirmed that this tetroxide is unstable due to the expected oxidation of its oxo ligands by the highly oxidizing platinum center.[102]

Many elements achieve their highest oxidation state in fluorides, such as RhF_6[104], PtF_6[44,105] and AuF_5[106], while other late binary TM fluorides such as PdF_6, AgF_4 and AuF_6 were only studied quantum-chemically.[107] In this work, we have attempted to yield another long-standing puzzled binary TM fluoride, molecular NiF_4 (OS(Ni) = IV), in noble gas matrices, which is unstable at ordinary conditions and of which no spectroscopic data has yet been reported.

The Oxo Wall Concept

Terminal oxo complexes of TM play a critical role in various chemical and biological processes. Early and medium transition metal species bearing terminal oxo ligands (O^{2-}) have been thoroughly investigated, *e.g.*, for nonheme $M^{IV/V}$=O (M = Fe, Mn) systems in catalysis and enzyme reactions.[108] However, tetragonal oxo complexes are rarely reported for TM complexes beyond group 8. Based on theoretical predictions this observation was explained by the so-called oxo-wall concept (Figure 1.5).[17] TM on the left side of this wall form stable oxo complexes, while oxo complexes of TM on the right are predicted to be unstable. The original prediction of the Oxo Wall is as follows: Octahedral TM oxo complexes with tetragonal symmetry can have no more than five *d* electrons to retain some MO multiple bonding. In the absence of π-bonding to the metal, the oxo ligand will be extremely basic and unstable with respect to protonation or attack by electrophiles.[17]

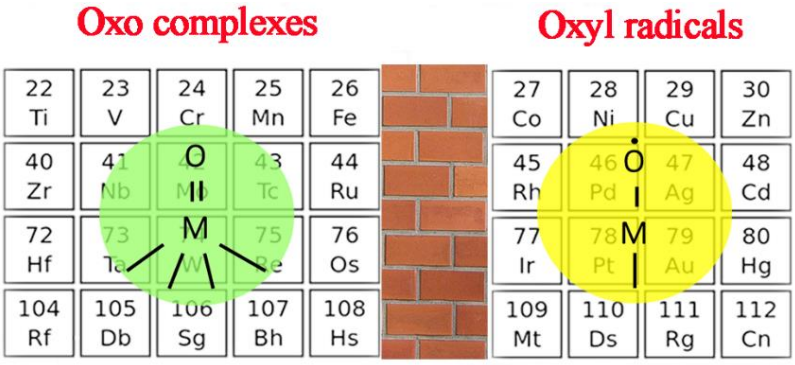

Figure 1.5. The oxo-wall between early and late transition metals.

Chemists continuously work on clarifying the mechanism behind the oxo-wall prediction. The requirements for forming stable oxo metal complexes are: i) Empty antibonding metal *d*-orbitals to allow strong π bonding to the oxo ligand, ii) a non-innocent oxo ligand that is not oxidized by the high-valent metal center. Due to the high *d*-electron count of late TMs, in particular of oxo complexes of group 11 and 10 metals, the molecular metal-type orbitals available for π-bonding to the oxo ligand are often fully or partially occupied. This weakens the metal-oxo bond. On the other side, the oxo ligand in high-valent late TM oxo complexes was shown not to be resistant to oxidation and preferentially forms partially

oxidized oxyl radical complexes ($O^{\bullet-}$, OS = –I) instead of oxido complexes with oxygen in the more common OS of –II.

The oxo wall concept is still controversial and some recent examples appear to challenge the oxo-wall concept, although they lack one of the requirements – the pseudo-octahedral coordination of tetragonal symmetry. The first compound, $Ir(O)(mes)_3$, has a distorted tetrahedral structure.[109] Other examples are terminal Co(III)-oxo,[110] Pt(IV)-oxo[18] and Pd(IV)-oxo[111] complexes. Another example is the platinum tungstate $K_7Na_9[Pt^{IV}(O)(H_2O)(PW_9O_{34})_2]$, which was suspected to contain a six-coordinated *trans*-Pt^{IV}(oxido)(aqua) dication with two $[PW_9O_{34}]^{9-}$ anions.[112] However, a later study revealed this previously assigned terminal Pt-oxo is actually $\{P_2W_{19}\}$ with small amounts of co-crystallized Pt(II).[13] Therefore, the Oxo Wall still stands and is actively reported in the literature.[113]

The Inverted Ligand Field

In a molecular orbital scheme, the overlap of two atomic orbitals generates one bonding orbital and one anti-bonding orbital.[114] There are three different cases: 1) when the energies of these two atomic orbitals are similar, the bond is covalent, and the contribution of the two atomic orbitals to the bonding and antibonding MOs is about 50%. 2) When the energy of the metal valence orbital is higher than that of the ligand orbital, the bond is predominantly ionic and the contribution of the metal orbital to the antibonding orbital is > 50%. 3) In cases when the energy of the ligand orbital is higher, the ligand field exerted by the ligands is inverted and the contribution of the ligand orbital to the antibonding orbital is > 50% (Figure 1.6).[38]

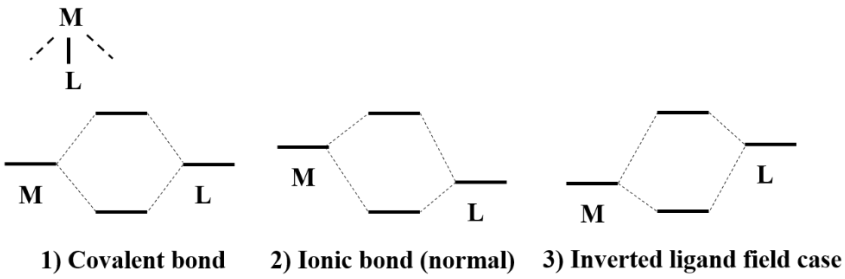

Figure 1.6. Simplified MO approach to covalent, ionic, and "inverted" bond types.

In MO schemes of most common transition metal complexes the orbitals of the ligands (Lewis bases) are lower in energy than those of the transition metal (Lewis acids) *d* orbitals. However, for the late *d*-block metals, due to the contraction of their *d* orbitals, these metal valence orbitals are closer to or even higher in energy than the *s* and *p* valence orbitals of the ligands. Consequently, more and more ligand-orbital character is displaying in the anti-bonding molecular orbitals. A well-known example is $[Cu(CF_3)_4]^-$,[38,115] its LUMO σ* orbital and also the π*-MOs show more ligand-orbital character rather than metal *d* character (Figure 1.7). However, not only the metal center can influence the chemical bonding, but also the donor abilities of ligands make a difference.[38] Moreover, it is intriguing to figure out the oxidation state of the central copper in such compounds. Unlike $[Ni(CO)_4]$ or $[Zn(NH_3)_4]$ system (18 valence electrons), the 16 valence electrons of $[Cu(CF_3)_4]^-$ must be divided into 10 valence electrons from Cu and 6 valence electrons from the ligands.[38,116] According to this analysis the central Cu(I) is surrounded by four $(CF_3)^{0.5-}$ ligands. The +I oxidation state of copper has been confirmed experimentally.[117]

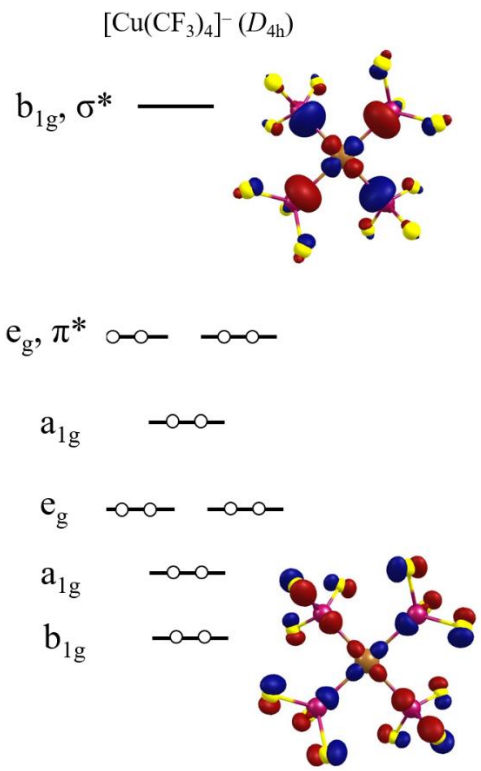

Figure 1.7. The partial molecular diagram of $[Cu(CF_3)_4]^-$ and selective orbitals (iso-surface = 0.08 electron a.u.$^{-3}$, B3LYP/cc-pVDZ).

Inverted ligand fields are often obtained with redox-active ("non-innocent") ligands.[54,98,118] Relevant to this work is the oxo ligand, which in most cases behaves as an innocent ligand that is described as a closed-shell dianionic oxido (O^{2-}, OS = –II) ligand. In high-valent late TM complexes, the oxo ligand becomes non-innocent as an oxyl radical $O^{\bullet-}$(OS = –I) due to a singly occupied molecular orbital contributed by the O-ligand. The term "non-innocent" is related to the ambiguous assignment of a formal metal oxidation state in such metal complexes.[118] In most cases the oxidation state of the metal center in such cases can not be clearly assigned.

Primogenic Repulsion and its Consequences for the 3*d* Elements

The orthogonality of shells can be ensured either by angular nodes (for shells with different l or m_l) or by radial nodes (for shells with same l and m_l). The radial notes ensure that the subshells ($(n$-1)*s*,*p*,*d*,*f*) stay orthogonal to the outermost orbitals (corresponding to *ns*,*p*,*d*,*f*), which moved outwards and become more diffuse. This was pointed out by Jørgensen[119] and coined the term "primogenic repulsion" by Pyykkö.[120] However, the 1*s*, 2*p*, 3*d* and 4*f* orbitals are special, since they have no core shell of the same angular momentum and thus lack a radial node. The absence of such radial nodes in orbital of the n-th shell ($n > 1$) leads to several consequences. For example, *np* orbitals tend to have larger radii than the corresponding *ns* orbitals, while the node-less 2*p* orbitals ($n = 2$) have a similar radial size as the 2*s* orbital (with one radial node).[121] The small 2*p* shell facilitates short and strong bonds in main group systems, but the opposite effect is observed in covalently bonded 3*d* transition metal compounds.[122] The valence 3*d* orbitals have a similar radial extent as the core 3*s*, 3*p* orbitals, due to the lack of a radial node of 3*d* orbitals. As a result, the Pauli repulsions between the filled core 3*s*, 3*p* orbitals and the ligand orbitals generally counteract an optimal overlap between the ligand orbitals and the 3*d* valence orbitals (Figure 1.8). This repulsion leads to the stretched covalent M−L bonds,[122] a smaller splitting between the bonding and antibonding orbitals than in a "non-stretched" case, which also partially explains why low-lying excited states are expected particularly in late 3*d* TM complexes.[122]

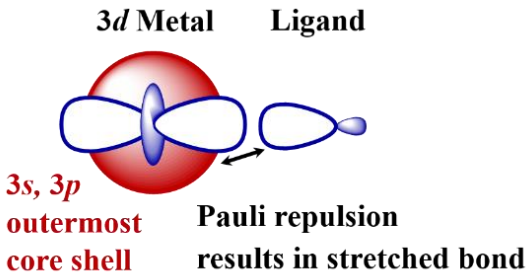

Figure 1.8. Schematic illustration of the weakening of the covalent overlap between a first-row transition metal 3*d* valence and ligand orbital (blue orbitals) by the Pauli repulsions between the metal core 3*s*,*p* shell (indicated by a red shell) and the ligand orbital.[122]

This bond-weakening effect is particularly relevant to high-valent late 3*d* TM compounds, such as the molecules $ONiF_2$, $OCuF_2$, NiF_3 and NiF_4, discussed in this thesis work. For predominantly ionic first-row TM fluorides MF_n the M–F bonds become shorter and stronger with increasing fluorination as a result of the increasing effective nuclear charge of the metal. Such an expected bond-shortening is well observed for *e.g.* the Fe–F bonds in the iron fluorides FeF_2 (r(Fe–F): 1.771 Å) > FeF_3 (1.758 Å) > FeF_4 (1.715 Å, see article [5.3]), but not for the more covalent Ni–F bonds in the binary fluorides NiF_2 (r(Ni–F): 1.718 Å), NiF_3 (1.722 Å), NiF_4 (1.700 Å). The bond-weakening with increasing fluorination of nickel is also shown by their decreasing Ni–F bond strength and the decreasing thermal stability of these fluorides (see article [5.3]).

References to Chapter 1:

[1] C. E. Elwell, N. L. Gagnon, B. D. Neisen, D. Dhar, A. D. Spaeth, G. M. Yee, W. B. Tolman, *Chem. Rev.* **2017**, *117*, 2059.

[2] Y. Shimoyama, T. Kojima, *Inorg. Chem.* **2019**, *58*, 9517.

[3] K. Ray, F. Heims, F. F. Pfaff, *Eur. J. Inorg. Chem.* **2013**, *2013*, 3784.

[4] Y. Gong, M. Zhou, L. Andrews, *Chem. Rev.* **2009**, *109*, 6765.

[5] K. A. Moltved, K. P. Kepp, *J. Phys. Chem. C* **2019**, *123*, 18432.

[6] S. Linic, H. Piao, K. Adib, M. A. Barteau, *Angew. Chem. Int. Ed.* **2004**, *43*, 2918.

[7] a) D.-A. Rosca, J. A. Wright, M. Bochmann **2015**, *44*, 20785; b) M. A. Cinellu, G. Minghetti, F. Cocco, S. Stoccoro, A. Zucca, M. Manassero, *Angew. Chem. Int. Ed.* **2005**, *44*, 6892.

[8] N. Gagnon, W. B. Tolman, *Acc. Chem. Res.* **2015**, *48*, 2126.

[9] V. A. Larson, B. Battistella, K. Ray, N. Lehnert, W. Nam, *Nat. Rev. Chem.* **2020**, *4*, 404.

[10] a) N. Dietl, C. van der Linde, M. Schlangen, M. K. Beyer, H. Schwarz, *Angew. Chem. Int. Ed.* **2011**, *50*, 4966; b) E. Rezabal, J. Gauss, J. M. Matxain, R. Berger, M. Diefenbach, M. C. Holthausen, *J. Chem. Phys.* **2011**, *134*, 64304.

[11] a) D. Schröder, M. C. Holthausen, H. Schwarz, *J. Phys. Chem. B* **2004**, *108*, 14407; b) N. J. Rijs, P. Gonzalez-Navarrete, M. Schlangen, H. Schwarz, *J. Am. Chem. Soc.* **2016**, *138*, 3125.

[12] T. R. Cundari, J. N. Harvey, T. R. Klinckman, W. Fu, *Inorg. Chem.* **1999**, *38*, 5611.

[13] K. P. O'Halloran, C. Zhao, N. S. Ando, A. J. Schultz, T. F. Koetzle, P. M. B. Piccoli, B. Hedman, K. O. Hodgson, E. Bobyr, M. L. Kirk et al., *Inorg. Chem.* **2012**, *51*, 7025.

[14] a) M. Zhou, R. H. Crabtree, *Chem. Soc. Rev.* **2011**, *40*, 1875; b) P. R. Sharp, *J. Chem. Soc., Dalton Trans.* **2000**, 2647.

[15] J. G. Smith, *Platinum Metals Rev.* **1988**, *32*, 84.

[16] M. Shelef, *Chem. Rev.* **1995**, *95*, 209.

[17] J. R. Winkler, H. B. Gray in *Molecular Electronic Structures of Transition Metal Complexes I* (Eds.: D. M. P. Mingos, P. Day, J. P. Dahl), Springer, Berlin, Germany, **2012**, pp. 17–28.

[18] E. Poverenov, I. Efremenko, A. I. Frenkel, Y. Ben-David, L. J. W. Shimon, G. Leitus, L. Konstantinovski, J. M. L. Martin, D. Milstein, *Nature* **2008**, *455*, 1093.

[19] I. Efremenko, E. Poverenov, J. M. L. Martin, D. Milstein, *J. Am. Chem. Soc.* **2010**, *132*, 14886.

[20] a) J. B. Mann, T. L. Meek, E. T. Knight, J. F. Capitani, L. C. Allen, *J. Am. Chem. Soc.* **2000**, *122*, 5132; b) M. Rahm, T. Zeng, R. Hoffmann, *J. Am. Chem. Soc.* **2019**, *141*, 342.

[21] W. T. K. Chan, W.-T. Wong, *Polyhedron* **2013**, *52*, 43.

[22] T. Schlöder, S. Riedel (Eds.) *Comprehensive inorganic chemistry II (Eds.: J. Reedijk; K. R. Poeppelmeier)*, Elsevier, Amsterdam, **2013**.

[23] W. Klemm, E. Huss, *Z. Anorg. Allgem. Chem.* **1949**, *258*, 221.

[24] M. J. Reisfeld, L. B. Asprey, R. A. Penneman, *J Mol. Spectrosc.* **1969**, *29*, 109.

[25] K. O. Christe, *Inorg. Chem.* **1977**, *16*, 2238.

[26] J. J. Lander, L. A. Wooten, *J. Am. Chem. Soc.* **1951**, *73*, 2452.

[27] H. Krischner, K. Torkar, B. O. Kolbesen, *J. Solid State Chem.* **1971**, *3*, 349.

[28] R. Gottschall, R. Schöllhorn, M. Muhler, N. Jansen, D. Walcher, P. Gütlich, *Inorg. Chem.* **1998**, *37*, 1513.

[29] G. Demazeau, *Z. Anorg. Allg. Chem.* **2005**, *631*, 556.

[30] P. Leszczyński, W. Grochala, *Acta Chim. Slov.* **2013**, *60*, 455.
[31] S.-T. Myung, K. Amine, Y.-K. Sun, *J. Power Sources* **2015**, *283*, 219.
[32] S. Möhle, M. Zirbes, E. Rodrigo, T. Gieshoff, A. Wiebe, S. R. Waldvogel, *Angew. Chem. Int. Ed.* **2018**, *57*, 6018.
[33] a) J. Suntivich, K. J. May, H. A. Gasteiger, J. B. Goodenough, Y. Shao-Horn, *Science* **2011**, *334*, 1383; b) R. S. McEwen, *J. Phys. Chem.* **1971**, *75*, 1782.
[34] P. Kalyani, N. Kalaiselvi, *Sci. Technol. Adv. Mater.* **2005**, *6*, 689.
[35] M. Merrill, M. Worsley, A. Wittstock, J. Biener, M. Stadermann, *J. Electroanal. Chem.* **2014**, *717-718*, 177.
[36] H. Chen, C. L. Freeman, J. H. Harding, *Phys. Rev. B* **2011**, *84*, 851081.
[37] M. Görlin, J. Ferreira de Araújo, H. Schmies, D. Bernsmeier, S. Dresp, M. Gliech, Z. Jusys, P. Chernev, R. Kraehnert, H. Dau et al., *J. Am. Chem. Soc.* **2017**, *139*, 2070.
[38] R. Hoffmann, S. Alvarez, C. Mealli, A. Falceto, T. J. Cahill, T. Zeng, G. Manca, *Chem. Rev.* **2016**, *116*, 8173.
[39] B. Zemva, K. Lutar, L. Chacón, M. Fele-Beuermann, J. Allman, C. Shen, N. Bartlett, *J. Am. Chem. Soc.* **1995**, *117*, 10025.
[40] M. Tramšek, B. Žemva, *Acta Chim. Slov.* **2002**, *49*, 209.
[41] a) M. Schmeisser, P. Sartori, *Chem. Ing. Tech.* **1964**, *36*, 9; b) N. V. Ignat'ev, U. Welz-Biermann, U. Heider, A. Kucheryna, S. von Ahsen, W. Habel, P. Sartori, H. Willner, *J. Fluorine Chem.* **2003**, *124*, 21; c) S. Mattsson, G. Senges, S. Riedel, B. Paulus, *Chem. Eur. J.* **2020**, Accepted paper.
[42] S. Riedel, M. Kaupp, *Coord. Chem. Rev.* **2009**, *253*, 606.
[43] a) N. Bartlett, D. H. Lohmann, *Proc. Chem. Soc.* **1960**, 14; b) B. G. Mueller, M. Serafin, *Eur. J. Inorg. Chem.* **1992**, *29*, 625.
[44] B. Weinstock, H. H. Claassen, J. G. Malm, *J. Am. Chem. Soc.* **1957**, *79*, 5832.
[45] R. Mitra, K.-R. Pörschke, *Angew. Chem. Int. Ed.* **2015**, *54*, 7488.
[46] H.-F. Klein, P. Kraikivskii, *Angew. Chem. Int. Ed.* **2009**, *48*, 260.
[47] A. Sivaramakrishna, H. S. Clayton, U. Muralikrishna, *J. Coord. Chem.* **2011**, *64*, 1309.
[48] F. D'Accriscio, P. Borja, N. Saffon-Merceron, M. Fustier-Boutignon, N. Mézailles, N. Nebra, *Angew. Chem. Int. Ed.* **2017**, *56*, 12898.
[49] N. M. Camasso, M. S. Sanford, *Science* **2015**, *347*, 1218.
[50] E. A. Meucci, N. M. Camasso, M. S. Sanford, *Organometallics* **2017**, *36*, 247.
[51] a) J. Cheng, L. Wang, P. Wang, L. Deng, *Chem. Rev.* **2018**, *118*, 9930; b) E. A. Meucci, N. M. Camasso, M. S. Sanford, *Organometallics* **2017**, *36*, 247.
[52] V. Dimitrov, A. Linden, *Angew. Chem. Int. Ed.* **2003**, *42*, 2631.
[53] M. Carnes, D. Buccella, J. Y.-C. Chen, A. P. Ramirez, N. J. Turro, C. Nuckolls, M. Steigerwald, *Angew. Chem. Int. Ed.* **2009**, *48*, 290.
[54] W. Kaim, *Eur. J. Inorg. Chem.* **2012**, *2012*, 343.
[55] S. N. MacMillan, K. M. Lancaster, *ACS Catal.* **2017**, *7*, 1776.
[56] J. T. Lukens, I. M. DiMucci, T. Kurogi, D. J. Mindiola, K. M. Lancaster, *Chem. Sci.* **2019**, *10*, 5044.
[57] J. R. Bour, N. M. Camasso, M. S. Sanford, *J. Am. Chem. Soc.* **2015**, *137*, 8034.
[58] J. S. Steen, G. Knizia, J. E. M. N. Klein, *Angew. Chem. Int. Ed.* **2019**, *131*, 13267.
[59] M. A. Domański, Ł. Wolański, P. Szarek, W. Grochala, *J. Mol. Model* **2020**, *26*, 52.
[60] F. Allouti, L. Manceron, M. E. Alikhani, *Phys. Chem. Chem. Phys.* **2006**, *8*, 448.

[61] a) O. Hübner, H.-J. Himmel, *J. Phys. Chem. A* **2012**, *116*, 9181; b) T. M. Ramond, G. E. Davico, F. Hellberg, F. Svedberg, P. Salen, P. Soederqvist, W. C. Lineberger, *J. Mol. Spectrosc.* **2002**, *216*, 1.
[62] T. P. Mangan, N. McAdam, S. M. Daly, J. M. C. Plane, *J. Phys. Chem. A* **2019**, *123*, 601.
[63] C. Wang, J. Jian, Z. H. Li, M. Chen, G. Wang, M. Zhou, *J. Phys. Chem. A* **2015**, *119*, 9286.
[64] R. Wei, Z. T. Fang, M. Vasiliu, D. A. Dixon, L. Andrews, Y. Gong, *Inorg. Chem.* **2019**, *58*, 9796.
[65] J. Cirera, E. Ruiz, S. Alvarez, *Inorg. Chem.* **2008**, *47*, 2871.
[66] L. Li, T. Stüker, S. Kieninger, D. Andrae, T. Schlöder, Y. Gong, L. Andrews, H. Beckers, S. Riedel, *Nat. Commun.* **2018**, *9*, 1267.
[67] a) R. Wei, Q. N. Li, Y. Gong, L. Andrews, Z. Fang, K. S. Thanthiriwatte, M. Vasiliu, D. A. Dixon, *J. Phys. Chem. A* **2017**, *121*, 7603; b) Y. Gong, L. Andrews, C. W. Bauschlicher, K. S. Thanthiriwatte, D. A. Dixon, *Dalton Trans.* **2012**, *41*, 11706.
[68] E. R. Batista, R. L. Martin, P. J. Hay, *J. Chem. Phys.* **2004**, *121*, 11104.
[69] H. M. Seip, *Acta Chem. Scand.* **1965**, *19*, 1955.
[70] M. Kimura, V. Schomaker, D. W. Smith, *J. Chem. Phys.* **1968**, *48*, 4001.
[71] L. H. Jones, S. Ekberg, *J. Chem. Phys.* **1977**, *67*, 2591.
[72] V. N. Bukhmarina, Y. B. Predtechensky, L. D. Shcherba, *J. Mol. Struct.* **1990**, *218*, 33.
[73] A. Miskowiec, A. E. Shields, J. L. Niedziela, Y. Cheng, P. Taylor, G. DelCul, R. Hunt, B. Spencer, J. Langford, D. Abernathy, *Physica B: Condensed Matter* **2019**, *570*, 194.
[74] a) J. R. Geichman, E. A. Smith, S. S. Trond, P. R. Ogle, *Inorg. Chem.* **1962**, *1*, 661; b) J. R. Geichman, E. A. Smith, P. R. Ogle, *Inorg. Chem.* **1963**, *2*, 1012.
[75] G. T. Seaborg, J. J. Katz (Eds.) *The Actinide Elements*, McGraw-Hill Book Company, New York, NY, **1954**.
[76] T. Vent-Schmidt, L. Andrews, S. Riedel, *J. Phys. Chem. A* **2015**, *119*, 2253.
[77] I. Norman, G. Porter, *Nature* **1954**, *174*, 508.
[78] E. Whittle, D. A. Dows, G. C. Pimentel, *J. Chem. Phys.* **1954**, *22*, 1943.
[79] F. Brosi, T. Vent-Schmidt, S. Kieninger, T. Schlöder, H. Beckers, S. Riedel, *Chem. Eur. J.* **2015**, *21*, 16455.
[80] L. Andrews, X. Wang, *Science* **2003**, *299*, 2049.
[81] a) T. R. Burkholder, L. Andrews, *J. Chem. Phys.* **1991**, *95*, 8697; b) L. B. Knight, B. W. Gregory, S. T. Cobranchi, D. Feller, E. R. Davidson, *J. Am. Chem. Soc.* **1987**, *109*, 3521.
[82] W. F. Howard, L. Andrews, *J. Am. Chem. Soc.* **1973**, *95*, 3045.
[83] E. S. Prochaska, B. S. Ault, L. Andrews, *Inorg. Chem.* **1977**, *16*, 2021.
[84] a) L. B. Knight, J. T. Petty, S. T. Cobranchi, D. Feller, E. R. Davidson, *J. Chem. Phys.* **1988**, *88*, 3441; b) H. A. Joly, J. A. Howard, *J. Phys. Chem. A* **1997**, *101*, 2817.
[85] W. Koch, M. C. Holthausen, *A chemist's guide to density functional theory*, Wiley-VCH, Weinheim, New York, **2001**.
[86] M. J. Frisch, G. W. Trucks, H. B. Schlegel, G. E. Scuseria, M. A. Robb, J. R. Cheeseman, G. Scalmani, V. Barone, G. A. Petersson, H. Nakatsuji, X. Li, M. Caricato, A. V. Marenich, J. Bloino, B. G. Janesko, R. Gomperts, B. Mennucci, H. P. Hratchian, J. V. Ortiz, A. F. Izmaylov, J. L. Sonnenberg, D. Williams-Young, F. Ding, F. Lipparini, F. Egidi, J. Goings, B. Peng, A. Petrone, T. Henderson, D. Ranasinghe, V. G. Zakrzewski, J. Gao, N. Rega, G. Zheng, W. Liang, M. Hada, M. Ehara, K. Toyota, R. Fukuda, J. Hasegawa, M. Ishida, T.

Nakajima, Y. Honda, O. Kitao, H. Nakai, T. Vreven, K. Throssell, J. A. Montgomery, Jr., J. E. Peralta, F. Ogliaro, M. J. Bearpark, J. J. Heyd, E. N. Brothers, K. N. Kudin, V. N. Staroverov, T. A. Keith, R. Kobayashi, J. Normand, K. Raghavachari, A. P. Rendell, J. C. Burant, S. S. Iyengar, J. Tomasi, M. Cossi, J. M. Millam, M. Klene, C. Adamo, R. Cammi, J. W. Ochterski, R. L. Martin, K. Morokuma, O. Farkas, J. B. Foresman, and D. J. Fox, *Gaussian 16*, Gaussian, Inc., Wallingford CT, **2016**.

[87] TURBOMOLE GmbH, *TURBOMOLE V7.3. a development of University of Karlsruhe and Forschungszentrum Karlsruhe GmbH*, **2018**.

[88] H.-J. Werner, P. J. Knowles, G. Knizia, F. R. Manby, M. Schütz, P. Celani, W. Györffy, D. Kats, T. Korona, R. Lindh, A. Mitrushenkov, G. Rauhut, K. R. Shamasundar, T. B. Adler, R. D. Amos, A. Bernhardsson, A. Berning, D. L. Cooper, M. J. O. Deegan, A. J. Dobbyn, F. Eckert, E. Goll, C. Hampel, A. Hesselmann, G. Hetzer, T. Hrenar, G. Jansen, C. Köppl, Y. Liu, A. W. Lloyd, R. A. Mata, A. J. May, S. J. McNicholas, W. Meyer, M. E. Mura, A. Nicklass, D. P. O'Neill, P. Palmieri, D. Peng, K. Pflüger, R. Pitzer, M. Reiher, T. Shiozaki, H. Stoll, A. J. Stone, R. Tarroni, T. Thorsteinsson, and M. Wang, *MOLPRO, version 2015.1, a package of ab initio programs*, **2015**.

[89] a) F. Neese, *WIREs Comput. Mol. Sci.* **2012**, *2*, 73; b) F. Neese, *WIREs Comput. Mol. Sci.* **2017**, *2*, e1327.

[90] a) C. Lee, W. Yang, R. G. Parr, *Phys. Rev. B* **1988**, *37*, 785; b) S. H. Vosko, L. Wilk, M. Nusair, *Can. J. Phys.* **1980**, *58*, 1200; c) A. D. Becke, *J. Chem. Phys.* **1993**, *98*, 5648.

[91] a) J. P. Perdew, *Phys. Rev. B* **1986**, *33*, 8822; b) A. D. Becke, *Phys. Rev. A* **1988**, *38*, 3098.

[92] a) K. L. Bak, J. Gauss, P. Jørgensen, J. Olsen, T. Helgaker, J. F. Stanton, *J. Chem. Phys.* **2001**, *114*, 6548; b) S. Coriani, D. Marchesan, J. Gauss, C. Hättig, T. Helgaker, P. Jørgensen, *J. Chem. Phys.* **2005**, *123*, 184107; c) D. Feller, K. A. Peterson, J. G. Hill, *J. Chem. Phys.* **2011**, *135*, 44102.

[93] a) W. Jiang, N. J. DeYonker, A. K. Wilson, *J. Chem. Theory Comput.* **2012**, *8*, 460; b) T. Schlöder, S. Riedel (Eds.) *Extreme Oxidation States of Transition Metals*.

[94] W. H. E. Schwarz, E. M. V. Wezenbeek, E. J. Baerends, J. G. Snijders, *J. Phys. B: At. Mol. Opt. Phys.* **1989**, *22*, 1515.

[95] a) P. Pyykkö, *Chem. Rev.* **1988**, *88*, 563; b) J. Autschbach, S. Siekierski, M. Seth, P. Schwerdtfeger, W. H. E. Schwarz, *J. Comput. Chem.* **2002**, *23*, 804.

[96] a) M. Douglas, N. M. Kroll, *Ann. Phys.* **1974**, *82*, 89; b) B. A. Hess, *Phys. Chem. A* **1985**, *32*, 756; c) B. A. Hess, *Phys. Chem. A* **1986**, *33*, 3742; d) G. Jansen, B. A. Hess, *Phys. Rev. A* **1989**, *39*, 6016; e) T. Nakajima, K. Hirao, *Chem. Rev.* **2012**, *112*, 385.

[97] a) Ch. Chang, M. Pelissier and Ph. Durand, *Phys. Scr.* **1986**, *34*, 394; b) E. van Lenthe, E. J. Baerends, J. G. Snijders, *J. Chem. Phys.* **1993**, *99*, 4597; c) S. Faas, J. G. Snijders, J. H. van Lenthe, E. van Lenthe, E. J. Baerends, *Chem. Phys. Lett.* **1995**, *246*, 632; d) E. van Lenthe, R. van Leeuwen, E. J. Baerends, J. G. Snijders, *Int J Quantum Chem* **1996**, *57*, 281.

[98] C. K. Jørgensen, *Oxidation numbers and Oxidation States*, Springer, Berlin, **1969**.

[99] L. S. Hegedus, *In Transition Metals in the Synthesis of Complex Organic Molecules*, University Science Books, Mill Valley, CA, **1994**.

[100] P. Karen, *Angew. Chem. Int. Ed.* **2015**, *54*, 4716.

[101] G. Wang, M. Zhou, J. T. Goettel, G. J. Schrobilgen, J. Su, J. Li, T. Schlöder, S. Riedel, *Nature* **2014**, *514*, 475.

[102] S. X. Hu, W. L. Li, J. B. Lu, J. L. Bao, H. S. Yu, D. G. Truhlar, J. K. Gibson, J. Marçalo, M. Zhou, S. Riedel et al., *Angew. Chem. Int. Ed.* **2018**, *57*, 3242.
[103] H. S. Yu, D. G. Truhlar, *Angew. Chem. Int. Ed.* **2016**, *55*, 9004.
[104] a) J. H. Holloway, E. G. Hope, G. Stanger, D. A. Boyd, *J. Fluorine Chem.* **1992**, *56*, 77; b) T. Drews, J. Supel, A. Hagenbach, K. Seppelt, *Inorg. Chem.* **2006**, *45*, 3782.
[105] a) B. Weinstock, H. H. Claassen, J. G. Malm, *J. Chem. Phys.* **1960**, *32*, 181; b) K. Seppelt, *Chem. Rev.* **2015**, *115*, 1296.
[106] X. Wang, L. Andrews, K. Willmann, F. Brosi, S. Riedel, *Angew. Chem. Int. Ed.* **2012**, *51*, 10628.
[107] a) R. Craciun, R. T. Long, D. A. Dixon, K. O. Christe, *J. Phys. Chem. A* **2010**, *114*, 7571; b) R. Craciun, D. Picone, R. T. Long, S. Li, D. A. Dixon, K. A. Peterson, K. O. Christe, *Inorg. Chem.* **2010**, *49*, 1056.
[108] a) B. S. Lane, K. Burgess, *Chem. Rev.* **2003**, *103*, 2457; b) E. M. McGarrigle, D. G. Gilheany, *Chem. Rev.* **2005**, *105*, 1563.
[109] R. S. Hay-Motherwell, G. Wilkinson, B. Hussain-Bates, *Polyhedron* **1993**, *12*, 2009.
[110] E. Andris, R. Navrátil, J. Jašík, M. Srnec, M. Rodríguez, M. Costas, J. Roithová, *Angew. Chem. Int. Ed.* **2019**, *58*, 9619.
[111] D. Munz, *Chem. Sci.* **2018**, *9*, 1155.
[112] T. M. Anderson, W. A. Neiwert, M. L. Kirk, P. M. B. Piccoli, A. J. Schultz, T. F. Koetzle, D. G. Musaev, K. Morokuma, R. Cao, C. L. Hill, *Science* **2004**, *306*, 2074.
[113] J. D. Rolfes, M. van Gastel, F. Neese, *Inorg. Chem.* **2020**, *59*, 1556.
[114] J. M. Mayer, *Comments Inorg. Chem.* **1988**, *8*, 125.
[115] G. Aullon, S. Alvarez, *Theor. Chem. Acc.* **2009**, *123*, 67.
[116] J. K. Burdett, *Inorg. Chem.* **1975**, *14*, 375.
[117] C. Gao, G. Macetti, J. Overgaard, *Inorg. Chem.* **2019**, *58*, 2133.
[118] C. K. Jørgensen, *Coord. Chem. Rev.* **1966**, *1*, 164.
[119] C. K. Jørgensen, *Ph.D. Thesis*, University of Copenhagen, Copenhagen, **1957**.
[120] P. Pyykkö, *Phys. Scr.* **1979**, *20*, 647.
[121] P. Pyykkö, *J. Chem. Res. Synop.* **1979**, 380.
[122] M. Kaupp, *J. Comput. Chem.* **2007**, *28*, 320.

2. Outline of this Thesis Work

2.1 Oxofluorides of Group 10 and Group 11 Transition Metals

The first molecular oxofluorides of group 11 and 10 TMs are described in articles [5.1] and [5.2]. In the first work we have shown that excited coinage metal atoms M (M = Au, Ag, Cu) react with OF_2 to yield the hypofluorites FOMF, as well as the elusive group 11 oxygen fluorides OAgF, OAuF, and OMF_2. The isolation of these novel species in rare-gas matrices allowed a direct spectroscopic investigation of these group 11 compounds bearing a terminal oxygen ligand. The linear molecules OAgF and OAuF have a $^3\Sigma^-$ ground state with a biradical character. Two unpaired electrons are accommodated in antibonding O−M π* orbitals. The computed spin density for triplet OAuF (Figure 2.1) of 1.34 at oxygen and of 0.53 at gold already indicates a partially inverted character of these singly occupied antibonding π* MOs, while the oxygen spin density of OCuF (1.08, reference [5.2]) corresponds to a predominantly covalent O=Cu bond. The linear OCuF is probably best described as $F^-Cu^{2+}O^{\bullet-}$, with the oxidation state of +II for copper and –I for oxygen.

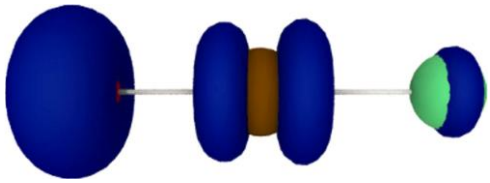

Figure 2.1. Computed Spin Density. Spin density iso-surface at 0.03 $Å^{-3}$ of OAuF calculated at the DFT B3LYP/AVTZ(-PP) level of theory.

For the $^2B_2$ ground state of the $OM^{III}F_2$ compounds only an O−M single bond arises, and a significant spin-density contribution was found at the oxygen atom as well. The high oxyl radical character of the terminal oxygen ligand in these group 11 fluorides is explained with an inverted ligand field.

The second work [5.2] presents our study on the linear oxo monofluorides OMF ($C_{\infty v}$) and the planar T-shaped oxo difluorides OMF_2 (C_{2v}) of the group 10 metal atoms M = Ni, Pd and Pt, as well as on the oxo trifluoride $OPtF_3$ (C_{2v}). These oxo fluorides were prepared by the reaction of the metal atoms with gaseous OF_2 and isolated in solid Ne and Ar matrices. These novel molecules were thoroughly investigated by a joint analysis of IR matrix-isolation spectroscopy and electronic structure calculations at the DFT, CCSD(T), as well as CASPT2 and MRCI levels of theory.

This work on novel oxofluorides of the metals of group 10 (article [5.2]) is divided into four parts. In the first part an overview is given about previous matrix-isolation and computational work on first-row TM oxofluorides. In the second part the results of our DFT and *ab initio* calculations on the target molecules are presented and in the third part the spectroscopic detection and the assignment of the experimental spectra is described.

These group 10 oxofluorides show terminal oxyl radical ligands with high spin densities of ≤ 1.0. In part four of reference [5.2] the oxyl radical character and the nature of the metal-oxo bond in late TM oxo complexes, especially the relationship between the electron population and the spin population on the oxo ligand in group 10 transition metal oxo and related compounds are discussed. According to a simplified three-electron π-bonding scheme the spin population at the oxo ligand increases with increasing covalence, and particularly with inversion of the M−O π-orbital space. For an isoelectronic

series including the linear triatomic group 9 metal difluorides F[9]F, the group 10 metal oxofluorides O[10]F, and the group 11 metal dioxides O[11]O (Figure 2.2) a continuous transition was observed from an ionic ligand field of the difluorides (F[9]F) via a predominantly covalent O=M bond in the oxo fluorides (O[10]F) to an inverted ligand field in the dioxides (O[11]O). The electron population of the metal *d*-orbitals increases continuously from the difluorides to the dioxides, while the spin density at the metal decreases. These observations indicate a decreasing effective oxidation number of the metals in these series that is accompanied by an increasing total spin density at the oxygen ligands, which in case of the dioxides is evenly distributed over both the oxygen atoms. This example illustrates the non-innocent behavior of the oxo ligand and the ambiguity of the assignment of metal oxidation states in these oxo compounds of late TM. Furthermore, a larger oxygen contribution to the π*-MOs results in an increased electrophilicity and a higher oxyl radical reactivity of the oxo ligand.

Also for the group 10 oxo difluorides OMF_2 the π*-MOs of are only moderately inverted and their high oxygen spin densities of > 1.0 can almost completely be attributed to the unpaired electrons accommodated in the π*-MOs. Remarkable differences were, however, found for the metal-oxygen bonds in the related oxo difluorides $ONiF_2$ and $OCuF_2$.

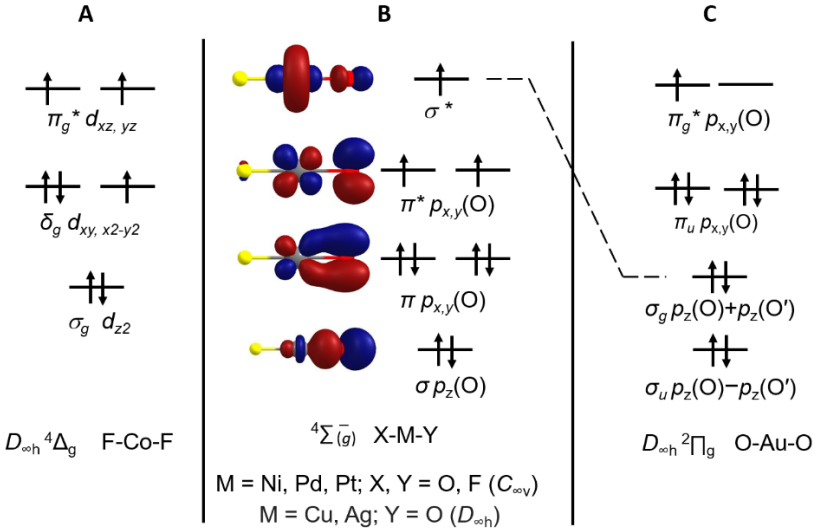

Figure 2.2. Qualitative orbital pattern and occupation scheme for the frontier orbitals of isoelectronic (d^7) linear group [9, 10 and 11] transition metal difluorides, dioxides, and oxo fluorides, XMY (X, Y = O, F). The configuration of OCuO ($^4\Sigma_g^-$, **B**) is similar to that of OAuO ($^2\Pi_g$, **C**) except the ordering of their σ_g MOs, which are connected by a dashed line in the figure.

2.2 The Molecular High-valent Nickel Fluorides NiF_3 and NiF_4

High-valent nickel fluorides are among the strongest known fluorinating and oxidizing agents, but there is a lack of experimental structural and spectroscopic investigations on molecular NiF_3 or NiF_4. Apart from their demanding synthesis, also their quantum-chemical description is difficult due to their open shell nature and low-lying excited electronic states. We provide the first spectroscopic characterization of molecular NiF_3 and NiF_4 in reference [5.3]. In this work distorted tetrahedral NiF_4 (D_{2d}) and trigonal planar NiF_3 (D_{3h}) molecules were produced by thermal evaporation and laser-ablation of nickel atoms in a fluorine/noble gas mixture and spectroscopically identified by a joint matrix-isolation and quantum-chemical study. Their vibrational band positions provide detailed insights into their molecular structures.

The rule of thumb that higher fluorides have shorter and stronger M−F bonds and correspondingly higher M−F stretching frequencies was not observed for the higher nickel fluorides. Our CCSD(T)/AVTZ

calculations predict a successive M–F bond shortening for the ionic iron fluorides FeF_n, with n = 1-4, and, albeit significantly weakened, also for CoF_n, n = 2-4, but the bond length in NiF_n, n = 2-4, remains almost unchanged. Another interesting result of this work is that the stretching fundamentals of the molecular trifluorides of M = Fe, Co, and Ni, which all adopt D_{3h} structures, appeared in a very narrow range between 743.6 cm^{-1} (Fe), 748.2 cm^{-1} (Co), and 743.8 cm^{-1} (Ni). A similar observation was observed for the tetrafluorides MF_4 of Fe to Ni, which also appears in a narrow spectral range (757 cm^{-1} (M = Fe), 767.8 (Co), 749.1 (Ni)).

These observations were traced back to the peculiar electronic structure of these late TM fluorides, such as high ionization energies, the occupation of M–F antibonding molecular orbitals, and the lack of the so-called "primogenic repulsion", caused by the absence of radial nodes in the wave functions of the 3*d* valence orbitals. Nickel is one of the most electronegative metallic elements. This implies a considerable covalent character of the Ni–F bonds, which increases with the oxidation state of nickel. Particularly for high-valent 3*d* TM complexes the similar radial extent of the 3*d* valence and the 3*p* core shell leads to a strong repulsion between the core 3*p* and the ligand valence electrons, which ultimately results in weakened metal-ligand bonds, a weak ligand-field, and the presence of several low-lying excited electronic (spin) states. Taken together, these factors not only pose a challenge to quantum-chemical predictions, and the unexpectedly low Ni–F stretching frequencies of these elusive high-valent molecular nickel fluorides were likely a major obstacle to their spectroscopic detection in previous studies.

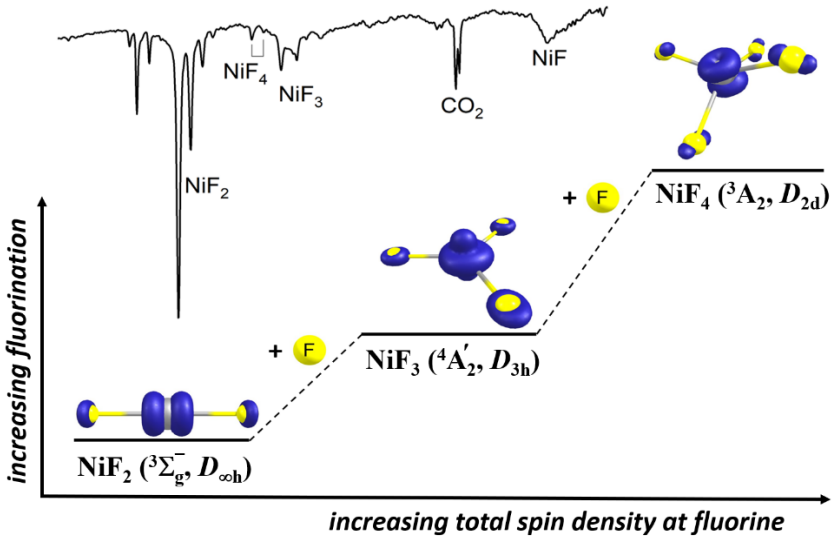

Figure 2.3. Molecular NiF_3 and NiF_4 are the missing tri- and tetrafluorides of the otherwise known binary first-row TM fluorides that are predicted to be stable. They are among the most powerful known fluorination and oxidation agents and the significant total spin density at the fluorine ligands of these species demonstrates their considerable fluorine radical character.

2.3 Infrared Spectra of Simple Actinide Molecules

In our work presented in work [5.4] infrared spectra and electronic structure calculations on the actinide compounds HAnX and H_2AnX_2 (An = U, Th; X = Cl, Br) are presented. The molecules were produced by the reaction of laser-ablated U and Th atoms with HCl and HBr and isolated in solid argon matrices. The computational predicted vibrational frequencies match our experimental observation very well. The most interesting trend is the experimental observation for the H–An stretching frequencies, which increases in the HAnF < HAnCl < HAnBr < HAn (An = U, Th) series. This observation is contra intuitive since a stronger electron withdrawing ligand is expected to strengthen the bond in the *trans* position.

However, the observed trend of the H−An stretching frequencies is consistent with an increase in the computed Mayer bond orders, as well as in the corresponding electron densities at the bond critical point obtained from an AIM calculation. It indicates an increase in the H−An bond strength going down the halogen families of the HAnX molecules. Additionally, the analysis of a Mulliken partition shows an increasing *f*-orbital participation in the H−An bonds of the HAnX (X = F < Cl < Br) molecules, while the opposite trend in the An−X bonds. Furthermore, the *f*-orbital participation is found to be larger for the Th analogues.

3. Publications

3.1 Investigation of Coinage Metal Oxo Fluorides

Oxygen Radical Character in Group 11 Oxygen Fluorides

Lin Li, Tony Stüker, Stefanie Kieninger, Dirk Andrae, Tobias Schlöder, Yu Gong, Lester Andrews, Helmut Beckers, Sebastian Riedel

Nat. Commun. **2018**, *9*, 1267. (Open Access)

https://doi.org/10.1038/s41467-018-03630-0

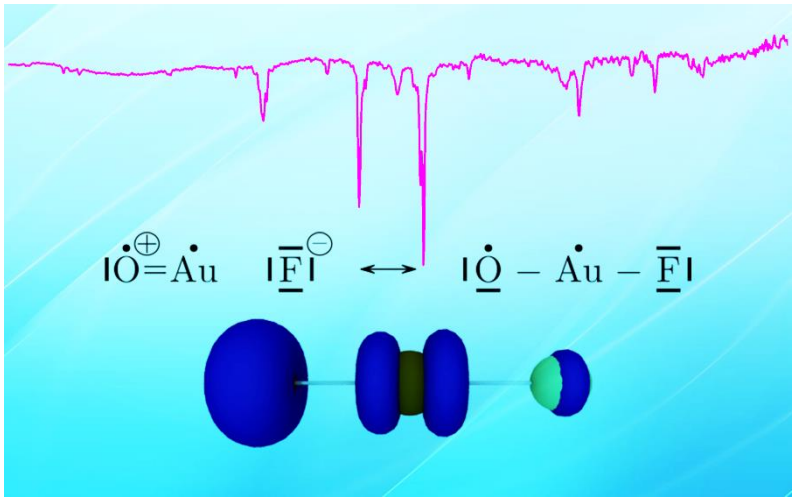

The computed spin density of linear molecule OAuF ($^3\Sigma^-$ ground state) shows a biradical character. Two unpaired electrons are located mainly at the oxygen ligand in antibonding M−O π* orbitals.

Author contribution

L. Lin carried out matrix-isolation experiments and collected data. L. Lin and H. Beckers wrote the manuscript. The quantum-chemical calculations were done by T. Stüker, S. Kieninger, D. Andrae and T. Schlöder. H. Beckers and S. Riedel managed the project and revised the manuscript.

Supporting Information

Oxygen Radical Character in Group 11 Oxygen Fluorides

The Pages 34-82 contain the supporting information were removed due to the Copyright.

The supporting information is available at

https://doi.org/10.1038/s41467-018-03630-0

3.2 Investigation of Group 10 Metal Oxo Fluorides

Molecular Oxofluorides OMF_n of Nickel, Palladium and Platinum: Oxyl Radicals with Moderate Ligand Field Inversion

Lin Li, Helmut Beckers, Tony Stüker, Tilen Lindič, Tobias Schlöder, Dirk Andrae, and Sebastian Riedel

Inorg. Chem. Front. **2021**, *8*, 1215.

https://doi.org/10.1039/D0QI01151G

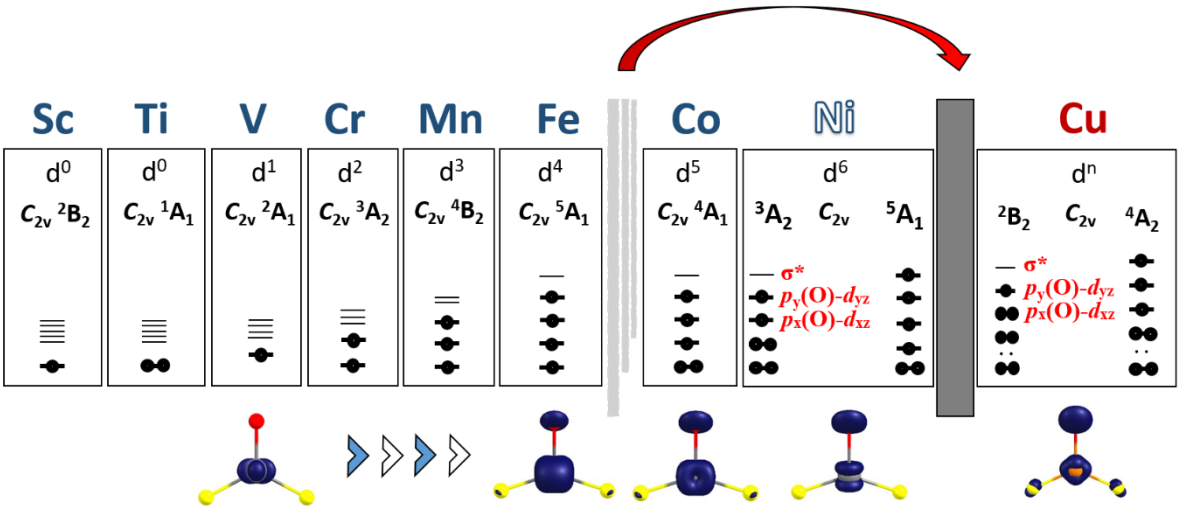

Qualitative orbital pattern and occupation scheme for the frontier orbitals of mononuclear first-row transition metal oxo fluorides OMF_2 (C_{2v}). The molecules are sketched in the *yz* plane (oxygen atoms marked in red, fluorine atoms in yellow). The orbitals are labelled by their most dominant metal 3*d* and ligand 2*p* atomic orbital contributions, where frontier orbitals with predominant oxygen 2*p* character are marked by red labels. Note that the given metal electron configuration d^n corresponds to the formal metal oxidation state and does not necessarily reflect the electronic structure of the metal complexes.

Author Contribution

L. Li and H. Beckers designed the project. L. Li carried out matrix-isolation experiments, did quantum-chemical calculations and wrote the manuscript. T. Lindič did the further calculations on nickel oxofluorides under the supervision of D. Andrae. T. Stüker did multi-reference calculations on nickel dioxofluorides. T. Schlöder did calculations on copper dioxofluorides. H. Beckers and S. Riedel revised the manuscript.

Supporting Information

Molecular Oxofluorides OMF_n of Nickel, Palladium and Platinum:

Oxyl Radicals with Moderate Ligand Field Inversion

The Pages 100-228 contain the supporting information were removed due to the Copyright.

The supporting information is available at

https://doi.org/10.1039/D0QI01151G

3.3 Investigation of Nickel Fluorides NiF_n (n = 1-4)

Searching for Monomeric Nickel Tetrafluoride: Unravelling Infrared Matrix Isolation Spectra of Higher Nickel Fluorides

Lin Li, Ahmed K. Sakr, Tobias Schlöder, Siri Klein, Helmut Beckers, Marios-Petros Kitsaras, Howard V. Snelling, Nigel A. Young, Dirk Andrae, and Sebastian Riedel

Angew. Chem. Int. Ed. **2021**, *60*, 6391. (Open Access)

https://doi.org/10.1002/anie.202015501

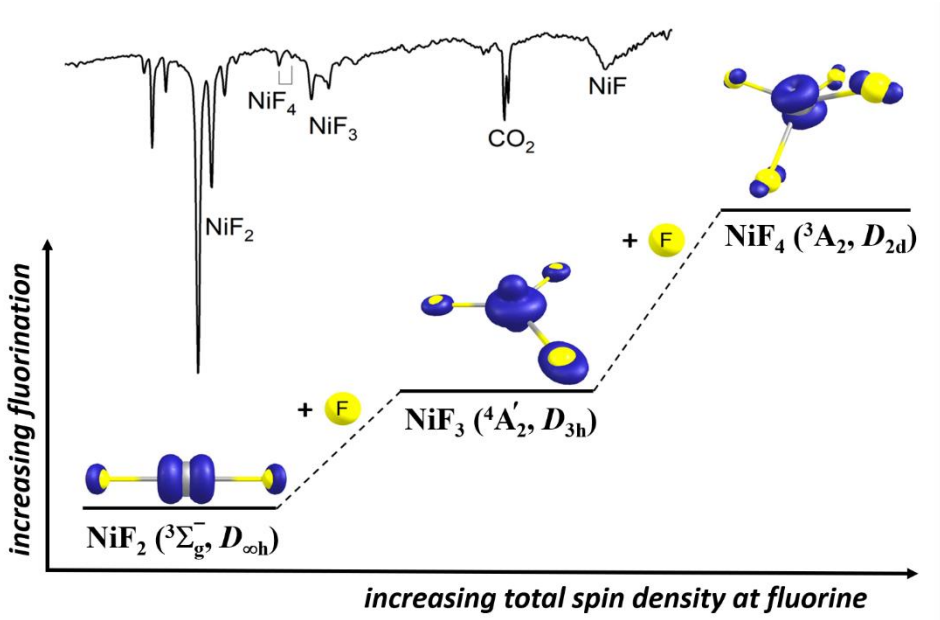

Molecular NiF_3 and NiF_4 are the missing tri- and tetrafluorides of the otherwise known binary first-row TM fluorides that are predicted to be stable. They are among the most powerful known fluorination and oxidation agents and the significant total spin density at the fluorine ligands of these species demonstrates their considerable fluorine radical character.

Author Contribution

L. Li carried out laser-ablation experiments and recorded infrared spectra, did quantum-chemical calculations, and wrote the manuscript. A. K. Sakr and H. V. Snelling did thermal experiments and recorded electronic absorption spectra under the supervisor of N. A. Young. M. -P. Kitsaras did part of calculations under the supervisor of D. Andrae. T. Schlöder and D. Andrae did calculations of nickel tetrafluoride. H. Beckers revised the manuscript. S. Riedel and N. A. Young managed the project and revised the manuscript.

Supporting Information

Searching for Monomeric Nickel Tetrafluoride: Unravelling Infrared Matrix Isolation Spectra of Higher Nickel Fluorides

The Pages 236-280 contain the supporting information were removed due to the Copyright.

The supporting information is available at

https://doi.org/10.1002/anie.202015501

3.4 Investigation of Uranium and Thorium Hydrides

Infrared Spectra of the HAnX and H_2AnX_2 Molecules (An = Th and U, X = Cl and Br) in Argon Matrices Supported by Electronic Structure Calculations

Lin Li,[+] Tony Stüker,[+] Lester Andrews, Helmut Beckers, and Sebastian Riedel

Chem. Eur. J. **2019**, *25*, 1795.

https://doi.org/10.1002/chem.201805372

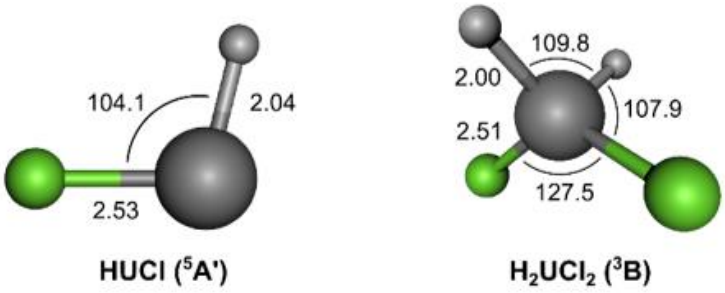

The structures calculated for HUCl and H_2UCl_2.

Author Contribution

L. Li and L. Andrews designed the project. L. Lin carried out laser-ablation experiments. T. Stüker did quantum-chemical calculations. L. Lin and T. Stüker wrote the manuscript (contributed equally to this work). L. Andrews and H. Beckers revised the manuscript. S. Riedel managed the project and revised the manuscript.

Supporting Information

Infrared Spectra of the HAnX and H_2AnX_2 Molecules (An = Th and U, X = Cl and Br) in Argon Matrices with Supported by Electronic Structure Calculations

The Pages 296-308 contain the supporting information were removed due to the Copyright.

The supporting information is available at

https://doi.org/10.1002/chem.201805372

4. Conclusion

The nickel fluorides NiF_n (n = 1-4), linear molecular OMF (M = Au, Ag, Ni, Pd and Pt), and T-shaped OMF_2 (M = Cu Ag, Au, Ni, Pd and Pt), as well as planer $OPtF_3$ oxyfluoride have been investigated by a combination of the matrix isolation technique, IR spectroscopy, and quantum-chemical methods. Electronic structure calculations were performed using single reference (DFT, CCSD(T)), and/or multi-reference methods (CASSCF, CASPT2), to provide ground state structures, vibrational frequencies, and spin populations of the novel molecules.

The linear molecular OMF have $^3\Sigma^-$ (M = Ag, Au) and $^4\Sigma^-$ (M = Ni, Pd and Pt) ground states with a biradical character. Their unpaired electrons reside in π* antibonding MOs, which results in weaker and especially for M = Au and Ag also in inverted π bonds. The oxo difluorides OMF_2 adopt a T-shape (C_{2v}) structure in their $^2B_2$ (M = Ag, Au) and $^3A_2$ (M = group 10) ground states. The oxo ligand in these molecules can also be considered as terminal oxyl radical. The electronic ground state of $ONiF_2$ [64] has been re-determined as $^3A_2$ based on the observation of an additional symmetric stretching vibration. In order to resolve the contradiction about the ground state of $OCuF_2$,[64,66] three near-degenerate electronic states (described as $^2B_2$, $^4A_2$-1, and $^4A_2$-2) were studied by CCSD(T) and CASPT2 calculations. The π-orbital spaces for the $^4A_2$-2 state and for the $^2B_2$ state of $OCuF_2$ are highly inverted. This results in a complete loss of O−Cu π-bonding and a high spin density at the oxo group. However, further experimental and computational studies of this molecule are needed as only the strongest IR active vibrational mode were detected in the experimental IR spectra. The analysis of the first row TM oxo fluorides OMF_2 indicates an increasing covalence of their O=M bond up to M = Ni. This bond finally becomes inverted for the group 11 TM, where the contributions of the O(2*p*) valence orbitals dominate the antibonding π*-MOs. Moreover, a computational study of isoelectronic, triatomic linear molecules, the group 9 metal difluorides F[9]F, group 10 metal oxo fluorides O[10]F, and group 11 metal dioxides O[11]O revealed that the effective metal oxidation state increases from the difluorides to the dioxides, which illustrates the non-innocent behavior of the oxo ligand in these late TM oxo fluorides and dioxides.

Molecular nickel tetrafluoride NiF_4 shows a distorted tetrahedral D_{2d} structure in the $^3A_2$ ground state. The two unpaired electrons are accommodated in two degenerated E-type orbitals. The planar trifluoride NiF_3 (D_{3h}) has a $^4A_2'$ ground state. Their IR spectroscopic data are reported for the first time. NiF_3 was produced by thermal evaporation and laser ablation of elemental nickel, as well as laser ablation of bulk NiF_2 in the presence of elemental fluorine diluted in rare gases. NiF_4 is likely formed in the solid noble gas matrices by the reaction of NiF_3 with photolytic produced fluorine radicals. With increasing fluorination (NiF_n, $n = 2 \rightarrow 4$), the spin population at the F ligand increases, and the Ni–F bonds become longer and weaker. Due to their appreciable fluorine radical character and weakened Ni–F bond strengths, these high-valent nickel fluorides are powerful fluorination and oxidation agents.

The actinide hydrogen halides HAnX and H_2AnX_2 (An = U and Th, X = Cl and Br) were produced by the reaction of laser-ablated U and Th atoms with HCl and HBr and characterized by their IR spectra in solid argon matrices and quantum-chemical methods. The H−An stretching frequencies increases in the order HAnF < HAnCl < HAnBr < HAn (An = U and Th), indicating an increase in the H−An bond strength going down the halogen families of the HAnX molecules. For the covalent H−An bonds also the *f*-orbital participation increases in the series HAnX, X = F < Cl < Br, while the opposite trend is found for the ionic An−X bonds.

5. List of Publications

Articles

[5.1] **Lin Li**, Tony Stüker, Stefanie Kieninger, Dirk Andrae, Tobias Schlöder, Yu Gong, Lester Andrews, Helmut Beckers and Sebastian Riedel, Oxygen Radical Character in Group 11 Oxygen Fluorides, *Nat. Commun*. **2018**, *9*, 1267.
https://doi.org/10.1038/s41467-018-03630-0

[5.2] **Lin Li**, Helmut Beckers, Tony Stüker, Tilen Lindič, Tobias Schlöder, Dirk Andrae, Sebastian Riedel, Molecular Oxofluorides OMF_n of Nickel, Palladium and Platinum; Oxyl Radicals with Moderate Ligand Field Inversion, *Inorg. Chem. Front.* **2021**, *8*, 1215.
https://doi.org/10.1039/D0QI01151G

[5.3] **Lin Li**, Ahmed K. Sakr, Tobias Schlöder, Siri Klein, Helmut Beckers, Marios-Petros Kitsaras, Howard V. Snelling, Nigel A. Young, Dirk Andrae, Sebastian Riedel, Searching for Monomeric Nickel Tetrafluoride: Unravelling Infrared Matrix Isolation Spectra of Higher Nickel Fluorides, *Angew. Chem. Int. Ed.* **2021**, *60*, 6391.
https://doi.org/10.1002/anie.202015501

[5.4] **Lin Li**,[+] Tony Stüker,[+] Lester Andrews, Helmut Beckers, Sebastian Riedel, Infrared Spectra of the HAnX and H_2AnX_2 Molecules (An = Th and U, X = Cl and Br) in Argon Matrices Supported by Electronic Structure Calculations, *Chem. Eur. J.* **2019**, *25*, 1795.
https://doi.org/10.1002/chem.201805372

[5.5] Hongmin Li, Helmut Beckers, **Lin Li**, Günther Thiele, Tony Stüker, Sebastian Riedel, Reactions of Titanium, Zirconium and Hafnium Atoms with Hydrogen Selenide: A Matrix-Isolation Study, *Chem. Phys. Lett.* **2020**, *740*, 137063.
https://doi.org/10.1016/j.cplett.2019.137063

Award

2019 Chinese-German Chemical Association (CGCA) Young Researchers Award Winner (The first class)

Conference Contributions – Poster Presentations

[1] **Lin Li**, Helmut Beckers, Tobias Schlöder, Marios-Petros Kitsaras, Dirk Andrae, Tilen Lindič, Sebastian Riedel, Fluorides and Oxygen Fluorides of Late Transition Metals in Matrix Isolation, *19th European Symposium on Fluorine Chemistry* **2019**, Warsaw, Poland.

[2] **Lin Li**, Tony Stüker, Dirk Andrae, Tobias Schlöder, Helmut Beckers, Sebastian Riedel, Group 11 Oxo Fluorides–Terminal Oxo Ligand gives rise to Intriguing Oxidation States, *GDCh Wissenschaftsforum Chemie* **2017**, Berlin, Germany.